AN EVALUATION OF THE EXPERIMENTAL HIGH-RESOLUTION RAPID REFRESH – ALASKA MODELING SYSTEM DURING WINTER 2017

by

Taylor Alexandria McCorkle

A thesis submitted to the faculty of
The University of Utah
in partial fulfillment of the requirements for the degree of

Master of Science

Department of Atmospheric Sciences

The University of Utah

December 2017

The University of Utah Graduate School

STATEMENT OF THESIS APPROVAL

The thesis of **Taylor Alexandria McCorkle**

has been approved by the following supervisory committee members:

John D. Horel	, Chair	**7/10/17** Date Approved
Thomas Reichler	, Member	**7/10/17** Date Approved
W. James Steenburgh	, Member	**7/10/17** Date Approved

and by **Kevin Perry** , Chair/Dean of

the Department/College/School of **Atmospheric Sciences**

and by David B. Kieda, Dean of The Graduate School.

ABSTRACT

The High-Resolution Rapid Refresh – Alaska (HRRR-AK) modeling system has been developed to provide high spatial (3 km horizontal) and temporal (0-36 hourly forecasts) guidance for weather conditions over Alaska. This study evaluated the experimental version of the HRRR-AK system available during the 2017 winter (December 2016 – March 2017) prior to its expected operational deployment by the National Centers for Environmental Prediction in early 2018. Of highest interest was to assess the model's ability to forecast the evolution, intensity, and timing of winter weather systems on the basis of surface pressure observations assimilated as part of its production cycle (e.g., from National Weather Service, NWS, stations) and those not assimilated (e.g., from USArray Transportable Array, TA, stations). Altimeter setting observations from the 100+ sites available from each of the NWS and TA networks are used to evaluate 138 complete 0- to 36-hour forecasts of altimeter setting initialized at 00 or 12 Universal Time Coordinated (UTC). More detailed examination of the forecasts using additional data assets was performed for the period 12-15 February 2017 during which a mid-tropospheric cut-off low over the Gulf of Alaska contributed to two distinct periods of strong downslope winds (southerly wind gusts in excess of 25 m s^{-1}) in the lee of the Alaska Range near Fort Greely in the Tanana Valley.

Throughout the 2017 winter, systematic differences in altimeter setting between the HRRR-AK analyses and the NWS assimilated (TA unassimilated) observations were

small (large). Upon removal of these initial biases from each of the subsequent 1- to 36-hour altimeter setting forecasts at the observation locations, the NWS and TA observations were found to be equally valuable for assessing forecast skill. When aggregated over the entire state, forecast errors were highest during the 12-15 February period within which the Gulf of Alaska cut-off low and Fort Greely downslope windstorms transpired. While the HRRR-AK analyses were quite useful for diagnosing the synoptic and mesoscale conditions during this period, the model forecasts tended to generate more intense surface pressure features rotating around the cut-off low and underestimated the abrupt increase in temperature during the first downslope windstorm and the intensity of the downslope winds during both events.

TABLE OF CONTENTS

LIST OF FIGURES

ACKNOWLEDGEMENTS

The completion of this master's thesis would not have been possible without the continued support and guidance of so many people. First, I would like to thank my advisor, Dr. John Horel, for not only advising me through the thesis process, but for encouraging me to attend workshops and conferences, answering any and all questions I may have, and of course for the constant support over the past two years. Since my arrival in Utah, each and every person in the Mountain Meteorology group has helped me in some way, whether it be fixing a coding problem, proof reading a paper, or just a friendly face through the tough times. Thank you all. I would also like to thank my committee, Dr. Thomas Reichler and Dr. Jim Steenburgh, for their help and support throughout the thesis process. I would also like to thank Dr. Trevor Alcott with NOAA ESRL for not only providing access to the HRRR-AK data, but for the many questions answered, conferences calls, and advice that made my thesis possible.

This work was supported by the National Science Foundation (NSF Grants 1252315 and 1443046) and a NOAA Collaborative Science, Technology, and Applied Research (CSTAR) Program Award (NA13NWS4680003). TA pressure data access was provided by the Incorporated Research Institutions of Seismology Web Services and the Array Network Facility at Scripps Institution of Oceanography, University of California San Diego. The University of Utah Center for High Performance Computing (CHPC) provided computational hardware and software necessary for completing this research.

CHAPTER 1

INTRODUCTION

Alaska's vast landmass spans more than 20 degrees of latitude, consists of 13 unique climate zones ranging from maritime to polar, and contains rugged topography at elevations from near sea level to Mt. Denali (6190 m), the highest point in North America (Searby 1968; Shulski and Wendler 2007; Shulski et al. 2010, Bienek et al. 2012, 2016). During Alaska's warm season (May-September), longer days and higher sun angles allow for enhanced surface heating that is conducive to unstable conditions, convection, and wildfires, especially in Alaska's interior (Grice and Comisky 1976; Reap 1991; Partain et al. 2016). Most climate regions in Alaska receive the bulk of their annual precipitation during the warm season, with the exception of some maritime and high-elevation locations (Shulski and Wendler 2007). The long interior Alaska cold season beginning in October is susceptible to year-to-year and longer-term variations, with increasing concerns regarding potential impacts of anthropogenic warming (Bienek et al. 2014; Cassano et al. 2016; Walsh et al. 2017).

The focus of this study is to examine synoptic and mesoscale conditions in Alaska during the 2017 winter season (hereafter defined as December 2016 through March 2017) using a mix of in-situ, remote sensing, and numerical weather prediction assets. The weather during a given cold season in Alaska is controlled largely by interactions

between planetary circulation features on time scales of weeks and months and the synoptic-scale weather systems embedded within them (Bieniek et al. 2012; Cullather et al. 2016). A number of planetary-scale signatures, or teleconnections, are known to affect Alaska during winter, e.g., the Arctic Oscillation (AO, Thompson and Wallace 1998) and the Pacific North American pattern (PNA, Papineau 2001; Bieniek et al. 2011). These low-frequency perturbations to the planetary-scale circulation modulate the development, progression, and demise of synoptic-scale features such as Aleutian Lows (Wilson and Overland 1986; Rodionov et al. 2007). Considerable attention has been placed on interannual and multiyear trends in the regional circulation over Alaska that have led to increasing temperatures and periods with anomalous warmth as seen during the 2015-16 winter (Shulski et al. 2010; Cassano et al. 2016; Walsh et al. 2017).

During December 2016, the regional circulation was characterized by the negative phase of the PNA and positive phase of the AO leading to ridging aloft over Alaska and a weakened Aleutian storm track. As the winter progressed, the magnitude of the AO teleconnection pattern weakened and the phase of the PNA became slightly positive, leading to a persistently weak wintertime storm track across the Aleutians and Gulf of Alaska. Figure 1.1a illustrates the 2017 winter departure of average sea level pressure from the 30-year climatological normal (1981-2010). Positive sea level pressure anomalies were situated over the Aleutian Islands, indicative of a subdued sub-polar circulation in the Gulf of Alaska (Pickart et al. 2009; Shulski et al. 2010). Seasonally averaged temperatures were cooler than normal for much of the state south of the Brooks Range, with warmer than normal conditions along the North Slope (Figure 1.1b). Further illustrating the complex relationship between regional circulation features and sensible

weather, a broad north-south swath of the state spanning several climate zones recorded 2-3 times their total monthly normal precipitation during January (Figure 1.1c) and other winter months (not shown).

The state of Alaska covers 1.718 million square kilometers of land, yet there are only approximately 150 automated weather stations supported by the National Weather Service (NWS) and the Federal Aviation Administration, generally at airports around the state. MesoWest (Horel et al. 2002) facilitates the monitoring of environmental conditions in Alaska at additional stations maintained by federal and state agencies, commercial firms, and the public. The data accessed, archived, and disseminated by MesoWest are made publicly available for near real-time viewing via web pages (e.g., mesowest.utah.edu and akff.mesowest.org) and for download via application programming interface (API) services (synopticlabs.org).

Surface weather observations available in Alaska by themselves are insufficient to characterize the evolution of weather conditions across the state during the 2017 winter. Numerical weather prediction systems that assimilate observations from diverse sources and provide guidance for Alaska have been relied upon for decades on the basis of global or regional model output (e.g., from the National Centers for Environmental Prediction, NCEP, Global Forecast System, or North American Mesoscale Forecast System, respectively). Currently, the operational model with the finest spatial (13 km) and temporal (hourly) resolution available for Alaska from NCEP is version 3 of the Rapid Refresh data assimilation/modeling system (RAPv3, Benjamin et al. 2016). Undergoing development by the RAP modeling team at the Earth System Research Laboratory is the Experimental High-Resolution Rapid Refresh – Alaska (HRRR-AK). This modeling

system uses 51 sigma levels in the vertical at a 3 km horizontal resolution nested within the larger domain of the RAPv3 (Figure 1.2). The HRRR-AK is initialized from the RAPv3 every 3 hours (0, 3, 6 Universal Time Coordinated, UTC, etc.) with hourly forecasts extending out to 36 hours.

The HRRR-AK will become operational during early 2018. It will be the first assimilation and forecast modeling system that encompasses Alaska with the temporal and spatial resolution necessary to resolve mesoscale weather features that impact Alaskans. Thus, there is considerable interest from model developers, researchers, and operational forecasters to assess its performance relative to the available data within the state. As a contribution compatible with other evaluations of the HRRR-AK currently underway by the model developers and researchers in Alaska, this study contrasts the model's ability to analyze and forecast the spatial and temporal evolution of surface pressure relative to surface pressure observations. These observations are from high-quality networks that were usually assimilated as part of the RAPv3 and HRRR-AK data assimilation systems as well as from those that were not included. The observations that are usually assimilated are from NWS stations, while those that are not included are part of EarthScope's USArray Transportable Array (TA), a research seismic monitoring network currently being deployed in Alaska. During the 2017 winter, the TA network consisted of over 100 active stations with installed microbarographs that continuously measure atmospheric pressure at a frequency of 1 Hz (Jacques et al. 2015; Jacques et al. 2016; Tytell et al. 2016; Jacques et al. 2017).

The HRRR-AK's ability to analyze and forecast at 1-hour intervals out to 36 hours for atmospheric surface pressure during the 2017 winter is evaluated for a number

of reasons. Sensor technologies allow accurate in-situ measurement of surface pressure and, ignoring spatial variations in the underlying topography for the moment, tend to be more representative of conditions over distances of tens of kilometers than near-surface temperature, moisture, or wind (Benjamin et al. 1999; Ancell 2012; Madaus et al. 2014). Reduction of surface pressure for higher elevation sites to pressure at sea level in terms of an altimeter setting is commonly employed to examine pressure gradients arising from weather features. Incorrect station elevation and imperfect assumptions about the air-temperature profile extrapolated downwards to sea level are generally the largest sources of error for applications of altimeter setting (Mohr 2004). Nonetheless, surface pressure and altimeter setting have been used extensively to diagnose the accuracy of numerical weather prediction model forecasts whether in terms of forecasting or tracking cyclones and anticyclones intensity, position, or evolution within the model domain (Colucci and Bosart 1979; Charles and Colle 2009; Mesquita et al. 2010; Wheatley and Stensrud 2010) or aggregate statistics over a portion or an entire model domain (Charles and Colle 2009; McMurdie and Casola 2009).

In addition to aggregate pressure statistics, a case study of a strong downslope wind event near Fort Greely during 12-15 February 2017 will be presented for which the forecast skill of the HRRR-AK was overall lower than other periods during the winter. In addition to strong winds in excess of 20 m s^{-1} during two successive days, air temperature increased by 35^{o}C in 36 hours in this region during the same period. The rapid warming and onset of the downslope windstorm allows for an evaluation of the model's forecasting ability on the mesoscale. Downslope windstorms in various locales in Alaska have been studied extensively (Murray 1956; Colman and Dierking 1992; Overland and

Bond 1993; Hopkins 1994; Nance and Colman 2000) as well as elsewhere in the continental United States and around the world. The approach taken in this research is to examine the ability of the HRRR-AK model analyses and forecasts to capture the spatial and temporal variability during this case study, rather than to attempt to improve the generally well-documented understanding of downslope windstorms in Alaska or elsewhere.

The deployment of the TA seismic network is the largest expansion of in-situ weather observing capabilities in Alaska in decades. The initial objective for this study was to demonstrate the potential of the TA network to examine mesoscale and synoptic-scale weather phenomena in Alaska. Since the network is not fully deployed yet, a secondary objective was sought that would take advantage of the network's current status. The maturing of the experimental HRRR-AK modeling system with a number of model updates completed during November 2016 opened the possibility to evaluate the accuracy of that modeling system for the winter as a whole as well as focus on the progression of major synoptic-scale systems across Alaska. However, not many of those types of weather disturbances were evident during the 2017 winter as a result of the prevailing planetary circulation during this period, so attention shifted to the 12-15 February 2017 downslope wind event as a means to examine in greater detail the model's performance when weather conditions were rapidly changing.

Hence, the objectives of this study are to illustrate:

1. The benefits of the deployment of the TA seismic network for weather-related research and operations; and

2. The HRRR-AK model performance in the aggregate for the entire 2017 winter as well as for the downslope wind storm event.

The characteristics of the TA network, other observational assets, and the HRRR-AK modeling system will be outlined in Chapter 2. Aggregate statistics for the 2017 winter season of the modeling system's accuracy as well as the case study of the 12-15 February 2017 downslope wind event follow in Chapter 3. Finally, in Chapter 4, a summary of this research and the work expected to continue as the TA array becomes fully deployed by the end of 2017 will be presented. That will include developing aggregate statistics for the summer 2017 season and examining the model treatment of the weather conditions associated with possible Alaskan wildfires during 2017 and later wildfire seasons.

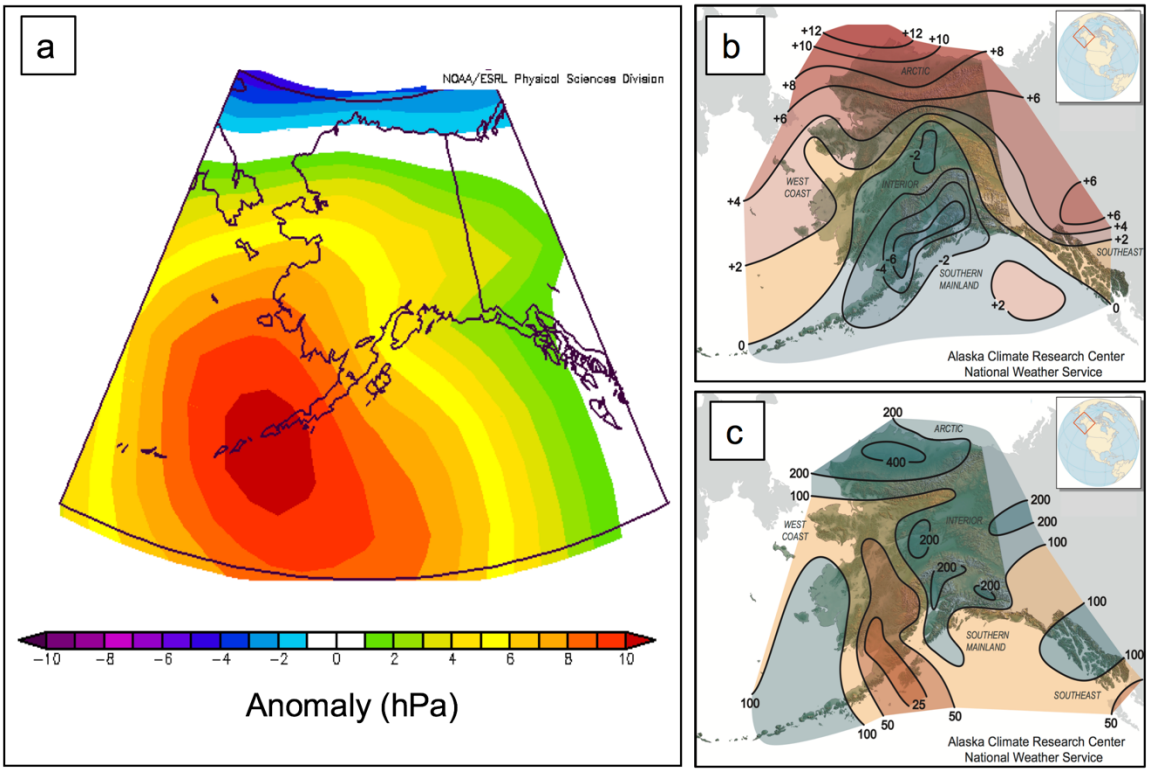

Figure 1.1. Winter 2017 summary figures showing (a) seasonal sea level pressure departure (hPa, shaded according to the scale) from the NCEP-NCAR Reanalysis climatology (1981-2010). (b) January 2017 temperature anomaly (° F) provided by the Alaska Climate Research Center. (c) January 2017 percent of normal monthly precipitation provided by the Alaska Climate Research Center.

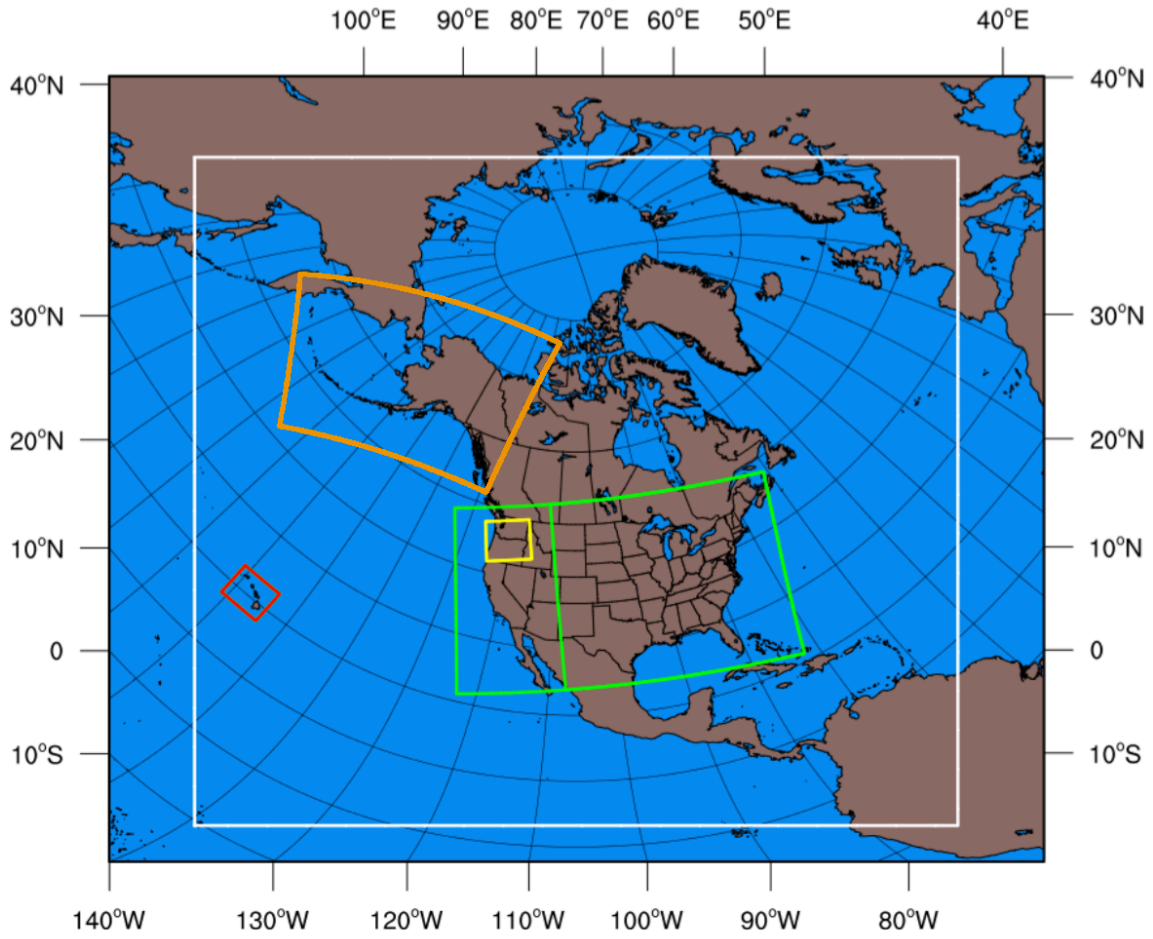

Figure 1.2. Horizontal domains for the Experimental HRRR-Alaska (orange), Experimental HRRR-Hawaii (red), Experimental HRRR nest Wind Forecast Improvement Project (yellow), HRRR (green), and RAPv3 (white).

CHAPTER 2

DATA AND METHODS

2.1 Meteorological Observations

In-situ and remotely sensed data platforms are used here to evaluate the HRRR-AK modeling system. All of the observations used for model validation, with the exception of the remotely sensed data, are accessed via MesoWest's API services.

2.1.1 National Weather Service (NWS) Stations

As shown in Figure 2.1a, there are currently 158 stations in Alaska operated by the NWS or under contract by the Federal Aviation Administration that generate hourly or sub-hourly reports of conventional meteorological variables (pressure, temperature, moisture, wind, etc.) in the form of Meteorological Terminal Air Reports (METAR). The METAR data are disseminated through various channels and usually are assimilated into the RAP and HRRR-AK models for forecast initialization. Generally, METAR reports are obtained in locales with small variations in terrain variability (surface roughness) as defined in Figure 2.1a by the standard deviation of surface elevation within the sample of the nine closest HRRR-AK model grid points.

2.1.2 USArray Transportable Array (TA) Stations

EarthScope's USArray TA is a research network of seismic monitoring stations deployed by the Incorporated Research Institutions for Seismology (IRIS). Beginning in 2004, this array of stations migrated eastward across the contiguous United States and is now being deployed as shown in Figure 2.1b across the state of Alaska in a quasi-grid with an average spacing of 85 km (Yang and Ritzwoller 2008; Pavlis et al. 2012; Jacques et al. 2015; Tytell et al. 2016).

Due to the impact that low-frequency, large-amplitude atmospheric acoustic signals have on measuring seismic activity, each TA station is equipped with a MicroElectro-Mechanical (MEMS) state-of-health barometer, an infrasound sensor, and a Setra-278 barometric pressure sensor (Tytell et al. 2016). The Setra-278 pressure sensor, which has better accuracy and resolution than the MEMS sensor, has a 1 Hz and a 40 Hz channel. Data from the 1 Hz channel are used in this study. EarthScope is currently deploying Vaisala WXT520 all-in-one weather sensors at many TA sites in order to expand the operational and research applications of the network (Tytell et al. 2016). Since few Vaisala sensors were deployed prior to the 2017 winter, data obtained from them will not be used in this study.

Since 1 March 2012, the pressure data from all TA stations has been obtained from IRIS, averaged over 5-minute intervals and made available to the public via MesoWest (Jacques et al. 2015). In addition, a web interface was designed specifically for the TA data, which displays current observations and has tools for filtering pressure perturbations and constructing time series (http://meso1.chpc.utah.edu/usarray/). Given the recognized quality of the USArray TA dataset, the atmospheric pressure data archive

described by Jacques et al. (2016) can also be accessed via the National Center for Atmospheric Research (NCAR) Research Data Archive (https://rda.ucar.edu/). All available data from the Vaisala all-in-one sensors are available via MesoWest as well.

The TA stations in Alaska are generally located in remote areas and often subject to harsh conditions. For example, Figure 2.2 shows a typical remote site with the Vaisala all-in-one sensor mounted on the roof of the small building. The terrain variability near the TA sites is often greater than that in the vicinity of the NWS/FAA stations (Figure 2.1). A mix of subjective and objective quality control checks have been applied to the Alaskan TA 1 Hz data that are similar to those used by Jacques et al. (2015). Subjectively, the data are checked using reports from the Array Network Facility, and if the data appear corrupt, are flagged. Objectively, data gaps longer than 5 minutes or pressure changes with a magnitude greater than or equal to 2 hPa per second are flagged. Flagged data are not deleted from the archive, but deemed suspicious and not used in this study. Despite the remote locations of many TA sites and lack of solar power during much of the period for the northernmost sites, only 12.2% of the total hourly observations were missing or failed quality control checks. For comparison, the NWS stations (generally electrically-powered and more accessible for routine maintenance and repair) had 12.3% missing or unusable data.

2.1.3 Remotely Sensed Data – NUCAPS

Remote sensing instruments are crucial for improving model forecasts, profiling trace gases in columns of the atmosphere, and obtaining near-surface observations in remote or data void areas (Lin et al. 2017). For this research, the Joint Polar Satellite

System Cross-Track Infrared Microwave Sounder Suite (CrIMMS) is used to retrieve environmental data records, such as vertical profiles of temperature and pressure, in non-precipitating conditions (Nalli et al. 2013). Part of the Suomi National Polar-orbiting Partnership, CrIMMS is a passive nadir sounder system comprised of Cloud-Cleared Radiances from the Cross-Track Infrared Sounder (CrIS) co-located with the Advanced Technology Microwave Sounder (ATMS) data (Smith et al. 2009; Nalli et al. 2013). The algorithms employed to derive the environmental data records used in this study are contained in the NOAA Unique CrIS/ATMS Processing System (NUCAPS Gambacorta et al. 2013). NUCAPS uses a "regularized least squares minimization" that solves for each variable individually while holding all others constant (Gambacorta et al. 2013; Nalli et al. 2013). The NUCAPS data used here were obtained via FTP in NetCDF4 format from NOAA's Comprehensive Large Array-Data Stewardship System (Liu et al. 2014).

2.2 HRRR-AK

The experimental 3 km HRRR-AK is nested within the 13 km domain of the RAP and uses the same data assimilation and physical parameterization schemes to produce analyses and forecasts (Benjamin et al. 2016). The RAPv3, implemented in spring 2016, employs the NOAA Gridpoint Statistical Interpolation (GSI) system for hourly data assimilation processing (Wu et al. 2002; Whitaker et al. 2008; Kleist et al. 2009). At each initialization time (t_0), the HRRR-AK uses initial conditions from the previous RAPv3 forecast cycle ($t_0 - 1\,hour$) interpolated to 3 km grid spacing for a 1-hour initial forecast. For each forecast, the boundary conditions are based off the RAPv3 forecast

cycle 3 hours prior to initialization time ($t_0 - 3\,hours$). A flow chart of the data assimilation process is shown in Figure 2.3. Similar to the RAPv3, the HRRR-AK currently uses the Weather Research and Forecasting (WRF) community regional model version 3.8 dynamical core (Skamarock et al. 2008). Given the WRF's non-hydrostatic capabilities, the HRRR-AK is run in the convection-permitting mode without a cumulus parameterization (Benjamin et al. 2016).

The HRRR-AK surface and pressure level gridded binary version 2 (grib2) files are downloaded locally via FTP and stored in an S3 archive along with the HRRR and continental United States experimental HRRR (Blaylock et al. 2017). Given the experimental status of the HRRR-AK during winter 2017, complete model runs are not available every 3 hours of every day. Over the 2017 winter season, 665, or 68.7%, of the analyses were available. The focus here is to examine those model runs for which the gridded data files have been available and archived for every forecast hour out to 36 hours. For example, 63% (52%) of the model runs initialized at 00 (12) UTC are complete. For each available analysis and forecast surface file, data from the grid points nearest to the NWS and USArray stations are extracted for comparison with the actual observations.

2.3 Analysis Methods

To focus on meteorologically relevant pressure variations and for consistency among the data sources, surface pressure from the TA stations and HRRR-AK grids are converted to altimeter setting. Altimeter setting observations at NWS stations are included in METAR reports. Conversion of surface pressure to altimeter setting requires

only surface pressure and station elevation assuming a temperature distribution below ground defined by the standard atmosphere (Bluestein 1992; Pauley 1998).

The HRRR-AK analysis and forecast surface pressure grids were converted to altimeter setting using surface pressure and elevation grids and the same standard atmosphere temperature profile used for the TA stations. Despite its 3 km grid spacing, the HRRR-AK's terrain field is still too coarse to accurately resolve Alaska's terrain for most locales (Figure 2.1). Even if the HRRR gridded surface pressure value exactly matches that observed by a TA station, discrepancies between the model grid elevation interpolated to the station location can lead to consistent differences between the model and station altimeter setting of ~1 hPa per 8 m difference in elevation. In order to focus on the model's ability to predict altimeter setting at the station locations, the difference at each station location between the analyzed and observed altimeter setting (referred to hereafter as the initial bias) is then subtracted from the subsequent model altimeter settings for each of the 36 hourly surface pressure forecasts. Thus, the "error" of the model's analyzed altimeter setting after removal of the initial bias is zero, and any discrepancies at later forecast times reflect model performance, not misrepresentation by the model of the actual terrain.

To examine sectors within the HRRR-AK's large domain (~3600 x 2800 km) that reflect areas of high interest to residents of Alaska, stations are grouped to examine the model's performance in those locales. The regions highlighted here are the Fairbanks – Tanana Valley region, which represents a continental climate, and the Anchorage – Alaskan Gulf region, which is a maritime-continental transition climate. Statewide and sub-regional aggregate statistical analyses of altimeter setting in terms of seasonal bias

and root mean squared error (RMSE) will be presented. In addition, a simple feature-tracking algorithm is used for a cyclone in the Gulf of Alaska during the period of the 12-15 February case study (Mesquita et al. 2010).

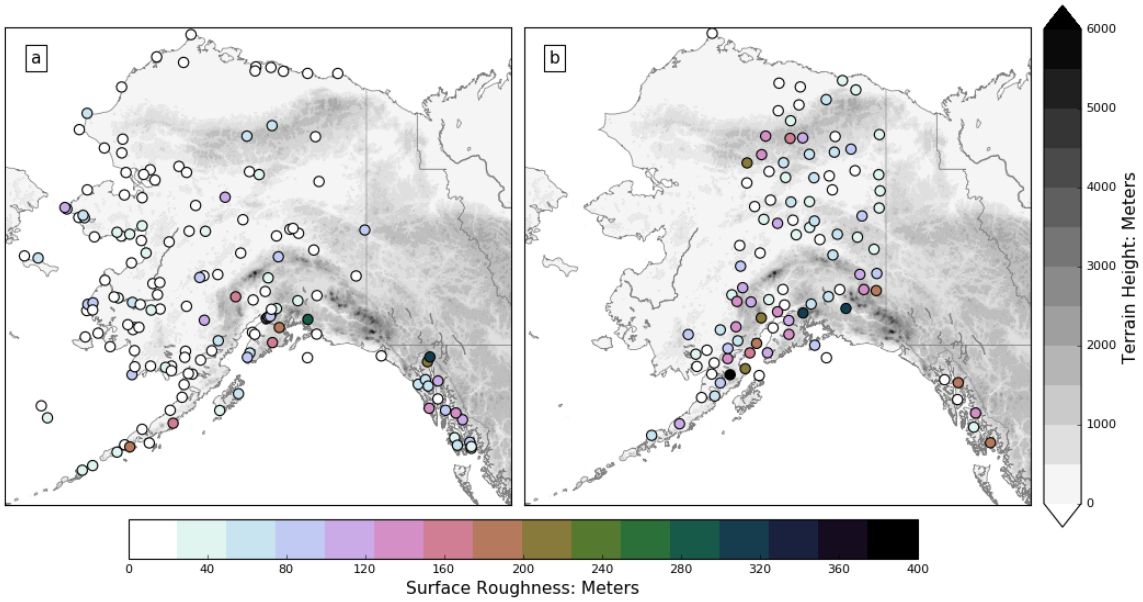

Figure 2.1. Surface roughness (m, circles shaded according to the scale at the bottom) defined as the standard deviation of HRRR-AK terrain values computed from the sample of the 9 closest grid points to: (a) NWS stations and (b) TA stations. Terrain height (m) of the Alaska-HRRR shaded in gray in both panels according to the scale on the right.

Figure 2.2. West-facing photograph of TA station (F24KX) south of the Brooks Range in northern Alaska. The small rock pile surrounds the vault containing the underground microbarograph and seismic instruments. The Vaisala all-in-one meteorological sensor is mounted on the pole on the top of the building.

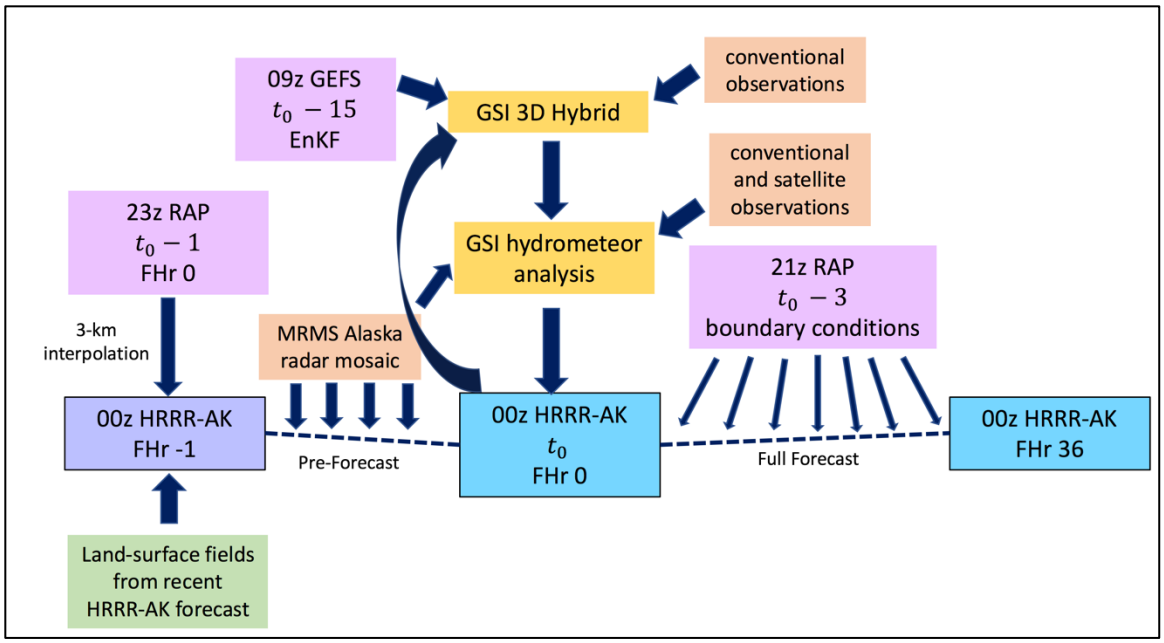

Figure 2.3. The data assimilation process for the initialization of each HRRR-AK model cycle.

CHAPTER 3

RESULTS AND DISCUSSION

3.1 Winter Aggregate Statistics

The 2017 Alaskan winter was marked by regional circulation features that produced a weakened Aleutian storm track, widespread above-average precipitation, and anomalous warmth along the North Slope of the Brooks Range. While large-amplitude cyclones did not traverse the state routinely, the 2017 winter period still proved valuable for a comprehensive model evaluation using the TA network and other resources. Since the TA network is still being deployed across the state, the NWS stations help increase the spatial coverage of this analysis as well as make it possible to compare model output to assimilated NWS to non-assimilated TA pressure observations.

As an illustration of the limitations arising from the reduction to altimeter setting for mountainous areas, Figures 3.1a and 3.1b display the 2017 winter season average altimeter setting from all available HRRR-AK analyses and average altimeter setting at the NWS and TA stations for those same times, respectively. The general increase in altimeter setting with latitude over the oceans is interrupted by lower altimeter setting values over high terrain, particularly for the Alaska and Brooks Ranges. Since the assumed standard atmosphere temperatures are higher than those applicable to Alaska's mountainous areas during winter, the reduction of surface pressure to sea level is

underestimated and the resulting altimeter settings are too low. Viewed over the model's entire domain, the winter-mean altimeter setting derived from the hourly NWS and TA observations are generally comparable to those obtained from the HRRR-AK analyses (Figure 3.1).

The initial biases of the HRRR-AK altimeter setting analyses for which complete 00 UTC model runs are available are shown in Figure 3.2a as a function of time during the 2017 winter relative to observations from the NWS and TA networks. Figure 3.2a highlights that the model's assimilation cycle used the pressure observations from the NWS stations during the winter and not the TA observations since the average initial biases relative to the NWS observations generally fall between 0.0 and -0.25 hPa, whereas the biases relative to the TA observations range within, and occasionally exceed, ±0.5 hPa. The average initial biases for the 12 UTC analyses exhibit similar tendencies to those evident in Figure 3.2 and are not shown. The average initial biases relative to the NWS observations do not exhibit much variability within the winter season, except for the positive biases evident during 18-22 January 2017. Model developer T. Alcott confirmed that surface observations were not assimilated into the HRRR-AK during that period (personal communication). The average initial bias for the TA network during that period is also higher; presumably since the assimilation cycle was not constrained by other surface pressure observations.

Figure 3.2b quantifies the average RMSE for each 00 UTC model run at forecast hour 36 after removing the initial bias and averaging over all available NWS and TA stations. RMSE values generally fluctuate between 2-6 hPa with no consistent differences between the RMSE computed at TA stations relative to NWS stations. There is also no

strong correspondence between model runs with higher initial biases leading to higher errors at hour 36. The highest 36-hour RMSE errors for the NWS stations are evident on 13-14 February, with the largest error during the winter for the TA stations on 14 February as well. This period will be examined in greater detail in section 3.2.

Spatial variations in the bias and RMSE of the HRRR-AK analyses and 36-hour forecasts computed from all complete 00 and 12 UTC model runs are shown in Figures 3.3 and 3.4 for NWS and TA stations, respectively. As expected from the time series of the initial biases computed over all of these stations for the 00 UTC runs (Figure 3.2), the initial biases at most NWS stations tend to be within ± 1 hPa (Figure 3.3a) while those at the TA sites are much larger (Figure 3.4a). Hence, the initial RMSE of the 00 UTC analyses are much smaller at the NWS stations (Figure 3.3b) compared to those at the TA sites (Figure 3.4b). After removal of the initial biases, average biases of 0 to -2 hPa for the 36-hour forecasts are evident at both the NWS and TA sites (Figures 3.3c and 3.4c), which indicate that the model loses mass over time. The 36-hour RMSE computed at the NWS and TA sites have comparable magnitudes of 2-3 hPa as well (Figures 3.3d and 3.4d). Hence, although the NWS pressure observations were assimilated and the TA observations were not, the pressure observations from both networks are equally valuable for assessing the model's performance once the initial biases derived from the differences between the analyses and observations are removed.

Selected TA stations in the Fairbanks – Tanana Valley and Anchorage – Gulf of Alaska regions (Figure 3.5a) are used to illustrate the altimeter setting errors as a function of forecast lead time averaged over all complete 00 and 12 UTC model runs (Figure 3.6). With initial biases removed, the average loss of mass with increasing forecast lead-time is

larger in interior Alaska (Figure 3.6a) compared to the Gulf of Alaska sites (Figure 3.6b). The small differences in the magnitudes of the RMSE relative to the bias in the interior (compare Figures 3.6a to 3.6b) suggest the pressure errors in the interior are dominated by the bias. However, larger RMSE than bias at longer lead times for the Gulf of Alaska sites (compare Figures 3.6c to 3.6d) suggest greater sensitivity to the forecast accuracy of the model's treatment of weather events traversing that region.

The results presented in this subsection highlight the aggregate behavior of the HRRR-AK surface pressure field as a function of period within the winter season, locale within Alaska, and forecast lead-time. Independent of whether the observations may have been assimilated (NWS) or not (TA), the aggregate statistics tend to be similar once the initial large differences in altimeter setting between the HRRR-AK analyses and TA observations are removed.

2.3 12-15 February 2017 Case Study

Prior to 12 February 2017, high surface pressures dominated the central and eastern Alaskan interior, contributing to the occurrence of clear skies and enhanced nocturnal radiational cooling over snow-covered surfaces, a strong stably-stratified boundary layer, and frigid surface air temperatures as low as -45°C in the area of the Tanana Valley, which is shown by the map in Figure 3.5b. Local conditions changed rapidly during the 12-15 February period, particularly in the Fort Greely area of the Tanana Valley immediately to the north of the Alaska Range. The changes in wind, temperature, and pressure in the Fort Greely area are highlighted in Figures 3.7-3.9 using observations at 5-minute intervals at both a TA site as well as from a local mesonet

maintained by the Fort Greely facility.

To provide context for the evaluation of the HRRR-AK analyses and forecasts across the model domain as well as locally, key observed characteristics in the Fort Greely area are summarized as follows:

- A steady increase in temperature from -30°C to -10°C from 18 UTC 12 February until 02 UTC 14 February followed by an abrupt 13°C increase in 10 minutes from 02:50 to 3:00 UTC 14 February (Figure 3.7b).
- Wind speeds were generally below 5 m s^{-1} until a rapid transition to sustained southerly winds in excess of 15 m s^{-1} from 3-10 UTC 14 February followed by a second period of sustained southerly winds in excess of 15 m s^{-1} from 21 UTC 14 to 5 UTC 15 February (Figure 3.7a).
- The first southerly downslope wind event (3-10 UTC 14 February) was characterized by warming temperatures and strong winds confined close to the lee of the upstream ridgeline of the Alaska Range (Figure 3.8a), while the second event, lasting from 21 UTC 14 February – 9 UTC 15 February, extended further north into the Tanana Valley, with above freezing temperatures throughout the Fort Greely area (Figure 3.8b).
- The pressure changes observed at the Fort Greely mesonet site (TCOA2) and the nearby TA site (K24KX) are nearly identical and include a 12 hPa drop in 12 hours from 6-18 UTC 13 February followed by another 9 hPa drop in the 10 hours prior to the lowest pressure of the period at 20 UTC 14 February (Figure 3.9).

Model runs that span this period are examined, in particular the forecasts initialized at 18 UTC 12 February extending out 36 hours to 6 UTC 14 February and

beginning at 18 UTC 13 February and continuing until 6 UTC 15 February. Figures 3.7 and 3.9 help to narrow the focus to the model's performance near TCOA2 and K24KX during this period, with the following insights:

- The model's localized warming trend after 18 UTC 12 February was too large, resulting in 10°C higher temperatures than observed at 12 UTC 13 February (Figure 3.7b). The abrupt warming associated with the onset of the first downslope wind event is missed by both model runs with the initialized temperatures at 18 UTC 13 February initially too high and then roughly comparable to those observed once the downslope wind event was underway.
- Surface winds at this location in Fort Greely remained light throughout the 18 UTC 12 February model run while the later forecast cycle underestimated the intensity of the downslope winds during both events by ~10 m s^{-1} (Figure 3.7a).
- Forecasted surface pressures were much too low (errors larger than 10 hPa) after 24 hours in both model forecast runs (Figure 3.9).

For decades, operational forecasters have recognized the difficulties to forecast these strong downslope wind events downstream of the Alaska Range, especially in the Tanana Valley (Murray 1956). The complex mix of synoptic-mesoscale interactions leading to the observed abrupt local changes and the extent to which the HRRR analyses and forecasts were able to resolve those interactions will be examined in the remainder of this subsection.

A deepening, mid-tropospheric trough characterized the synoptic weather pattern near Alaska on 12 February 2017 over western Alaska that plunged southward into the Gulf of Alaska by 14 February, while an upper-level ridge situated over the Northwest

Territories of Canada remained relatively stationary. Figures 3.10a and 3.10c show mid-tropospheric conditions at 12 UTC 13 February and 12 UTC 14 February, respectively. The shortwave trough, evident from the low temperatures and strong winds embedded on the western edge of the larger-scale cut-off low on the 13th (Figure 3.10a), progressed southward and deepened the cut-off low located south of the Aleutian Islands by 12 UTC on the 14th (Figure 3.10c). Strong warm-air advection in the mid-troposphere and the strongest 700 hPa winds on the eastern periphery of the cut-off low shifted northward across the Alaska Range during this 24-hour period. Later, the embedded shortwave continued to spin within the cut-off low leading to a shift in the trough axis from southwest-northeast at 12 UTC 14 February to south-north by 12 UTC 15 February (not shown).

As mentioned related to Figure 3.2b, some of the largest 36-hour forecast errors during the winter were observed during this period. The skill of the 18-hour forecasts for the mid-tropospheric (700 hPa) conditions valid at 12 UTC 13 February and 12 UTC 14 February is shown in Figures 3.10b and 3.10d. Overall, the 18-hour forecasts are quite good at capturing the general sense of the prevailing synoptic situation at these times, although the 18-hour forecast valid at 12 UTC 13 February tended to deepen the cut-off low too much by that time (Figure 3.10b) and the later model run at 12 UTC 14 February shifted the cut-off low somewhat further west than analyzed (Figure 3.10d). While the 700 hPa temperature gradients in the forecasts are reasonably close to those analyzed, the forecasted southerly 700 hPa winds impinging into southern Alaska and across the Alaska Range upstream of Fort Greely are ~5-10 m s^{-1} too strong, which leads to excessive mid-tropospheric warming in the forecasts at these two times.

Mid-tropospheric air temperatures derived by the NUCAPS algorithm from CrIMSS radiance data are evaluated as a means to validate synoptic-scale features in the HRRR-AK analyses and forecasts. A key reason for examining the NUCAPS data is that they are not assimilated by the RAPv3 or HRRR-AK forecast systems (Lin et al. 2017). Initial examination of NUCAPS vertical temperature profiles in the Fort Greely area relative to the HRRR-AK model's analysis soundings showed large discrepancies within the lowest 100 hPa, which suggested that the NUCAPS boundary layer temperatures were not realistic, particularly for the strongly stratified conditions (not shown). Shifting to the scale of the entire HRRR-AK domain, Figure 3.11 illustrates the swaths within which the NUCAPS data are available at 12 UTC 13 February 2014. Differences between the HRRR-AK and NUCAPS 500 hPa and 700 hPa temperature are superimposed on the HRRR-AK analyses and forecasts in the panels. Discrepancies between the 500 hPa temperature analysis and NUCAPS data (Figure 3.11a) are much smaller than those at 700 hPa (Figure 3.11c). The spatial patterns for the differences from 18-hour forecasts initialized at 18 UTC 12 February (Figures 3.11b and 3.11d) are nearly identical to those computed from the analyses with the largest errors evident above elevated terrain. Hence, the NUCAPS data are likely better suited for defining the atmospheric state above 700 hPa. For example, it is not possible to ascertain whether the lower NUCAPS 700 hPa temperatures than the HRRR-AK analyses or forecasts in the vicinity of the Alaska Range reflect the actual conditions in that region, particularly since the terrain elevation is near or above that level at many spots. Table 3.1 summarizes the RMSE differences between the analyses and forecasts relative to the NUCAPS data at 500, 700, and 850 hPa for analyses and 18-hour forecasts valid at 12 UTC 13 February

and 14 February. While the high RMSE values at 850 hPa reflect in part that this level is below ground in portions of the domain, the discrepancies are so large that it can be concluded more generally that the NUCAPS data are not suitable for model validation at that level and that may also be true for 700 hPa temperature over much of Alaska.

Figure 3.12 illustrates the evolution of surface pressure during this event in terms of the 3-hour change in altimeter setting observed at TA stations and forecasted by the HRRR-AK at lead times of 12 hours (Figures 3.12a and 3.12c) and 24 hours (Figures 3.12b and 3.12d). From 9-12 UTC 13 February (Figure 3.12a), pressures were observed to fall at many TA stations, but the 12-hour HRRR-AK forecasts appeared to be lowering the pressures more than that observed, particularly to the west of the Alaska Range. This is the time period when forecasted pressures were falling too rapidly in the Fort Greeley area as well (Figure 3.9). The 3-hour pressure falls at the NWS stations also tend to be smaller than those forecasted in that region of western Alaska (not shown). For the 3-hour period ending at 00 UTC 14 February (Figure 3.12b), the north-south cross-barrier pressure gradient across the Alaska Range is enhanced as a result of increasing pressure in the vicinity of Anchorage- Kenai Peninsula area and nearly steady pressures to the north of the Range (see also Figure 3.9). The 24-hour forecast of pressure tendencies valid at that time are dropping the pressures too much further north at that time. Subsequent falling pressures forecast in that region between 9-12 UTC 14 February (Figure 3.12c) may reflect the model forecast's overly strong warm-air advection aloft (Figure 3.10d) followed by pressure rises by 00 UTC 15 February (Figure 3.12d) as the embedded short-wave trough continued its counterclockwise spin within the cut-off low.

The amplitude of the pressure rises forecasted at 00 UTC 15 February by the HRRR-AK to the south of the Alaska Range is stronger than those observed.

For this case study, an objective feature tracking method was used to evaluate the ability of the HRRR-AK to forecast the cyclone's track, intensity, and evolution over the Gulf of Alaska. Altimeter setting data over land were not used due to the systematic errors over land arising from reduction to sea level evident in Figure 3.1. The analyzed track at 3-hour intervals from 00 UTC February 13 to 00 UTC February 15 2017 is shown in Figure 3.13. For reference, the HRRR-AK altimeter setting analyses at 00 UTC 14 February and 09 UTC 14 February are shown in Figures 3.13a and 3.13b, respectively. In addition, Figure 3.14 shows the change in magnitude of the surface low during this period. From 00 UTC – 09 UTC 13 February, the surface low deepened by a few hPa (Figure 3.14) and tracked northward (Figure 3.13). From 09 UTC 13 February until 6 UTC 14 February, the surface low could be best described as an elongated north-south oriented trough (Figure 3.13a) that was slightly weakening in amplitude (Figure 3.14). While the objectively-defined track jumps westward from 06 UTC to 09 UTC 14 February, the 3-hourly sequence of HRRR-AK analyses shows the development of the secondary low further west evident in Figure 3.13b that began to develop at 06 UTC and then deepened and tracked northward towards Kodiak Island through 18 UTC. The 3-hour pressure falls evident in Figure 3.8c between 9-12 UTC in the Howe Sound area are a reflection of the development and northward movement of this second low. The forecasted tracks of the surface low initialized from both the 00 UTC and 12 UTC 13 February emphasized the position of the north-south oriented trough to the south of the Katmai Peninsula region in rough agreement with its analyzed position (Figure 3.13).

Both model runs deepened the central pressure of that trough too much over time through 09 UTC February 14 and did not develop the second low further west (Figure 3.14).

Returning to the Fairbanks-Tanana Valley area (Figure 3.5b), the mesoscale structure evident in the HRRR-AK analyses and forecasts of surface air temperature and 10 m wind between 12 UTC 13 February and 00 UTC 15 February are examined in Figures 3.15-3.17. Figures 3.15a and 3.16a display analyses of vector winds and the 10 m wind gust and 2 m air temperature, respectively, before the onset of the first downslope windstorm. Strong wind gusts were analyzed to be confined to the higher elevations (Figure 3.15a), contrasting with the calm winds and colder temperatures at the valley floor (Figure 3.16a), and temperatures below -20°C persisting near Fairbanks. At 03 UTC 14 February, the HRRR-AK analyses highlight the development of the localized downslope winds and higher temperatures in the lee of the Alaska Range including the Fort Greely area (Figures 3.15b and 3.16b). Easterly winds down the Tanana Valley and higher temperatures over the elevated terrain to the north of the Tanana Valley are evident as well. Wind speed and gust forecasts at lead times of 33 h (Figure 3.15c) and 9 h (Figure 3.15d) valid at 03 UTC 14 February hint at enhanced winds in the lee of the Alaska Range, but the magnitude of the sustained winds and gusts is much too low. Additionally, the 33-hour and 9-hour 2 m temperature forecasts valid at 03 UTC 14 February produced widespread warming (Figures 3.16c and 3.16d, respectively), which was not observed or analyzed (Figure 3.16b).

Between the two downslope wind events (12 UTC 14 February), the low-lying areas within the upper Tanana Valley warmed slightly compared to the day before, but calm winds and temperatures below -20°C temperatures remained near Fairbanks (Figure

3.17a). Prior to 00 UTC 15 February, the second and more widespread period of downslope winds developed (Figure 3.17b). The HRRR-AK 30-hour and 6-hour forecasts, shown in Figures 3.17c and 3.17d, respectively, were better at predicting the strength and spatial extent of the second downslope wind event when compared to the first event. However, the 30-hour forecast indicated very high wind speeds over the higher terrain of the Alaska Range (Figure 3.17c) leading to more widespread warming than that analyzed associated with the mixing downward of the larger-scale warm air advection prevailing at this time aloft (Figure 3.17b).

Table 3.1: Temperature RMSE (°C) of HRRR-AK analyses at 12 UTC 13 and 14 February and 18-hour forecasts valid at those times at 850, 700, and 500 hPa computed relative to all of the available NUCAPS profiles in Figure 3.11.

Level	**12 UTC 13 February Analysis**	**18-h Forecast Initialized at 18 UTC 12 February**	**12 UTC 14 February Analysis**	**18-h Forecast Initialized at 18 UTC 13 February**
500 hPa	1.66	1.57	1.65	1.73
700 hPa	3.48	3.34	3.86	3.94
850 hPa	4.68	4.02	7.51	7.70

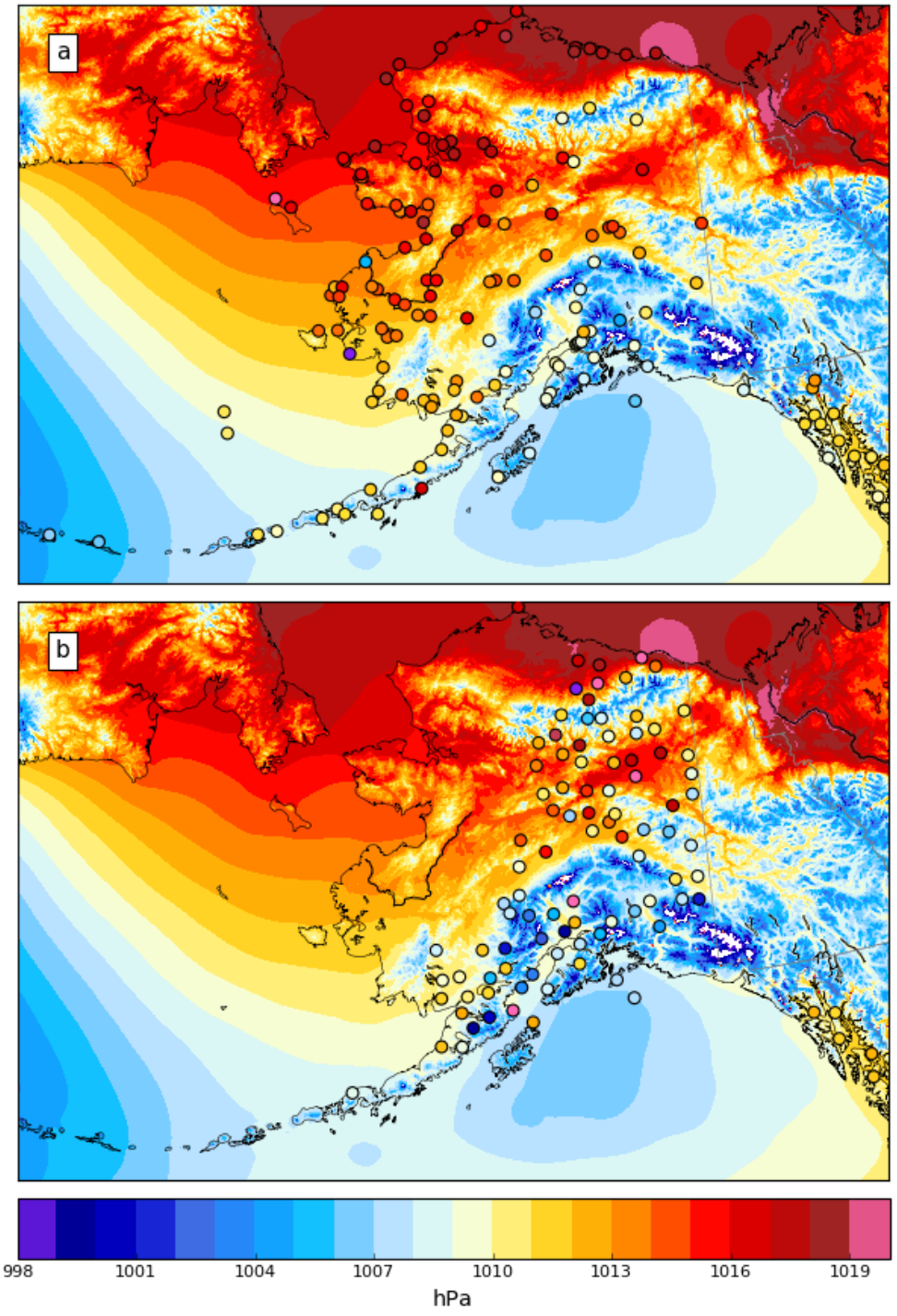

Figure 3.1. Winter 2017 average altimeter setting (hPa) derived from all available HRRR-AK analyses shaded in both panels according to the scale at the bottom with average altimeter setting (hPa), (circles shaded according to the scale at the bottom) for the same times computed from: (a) all NWS stations and (b) all TA stations.

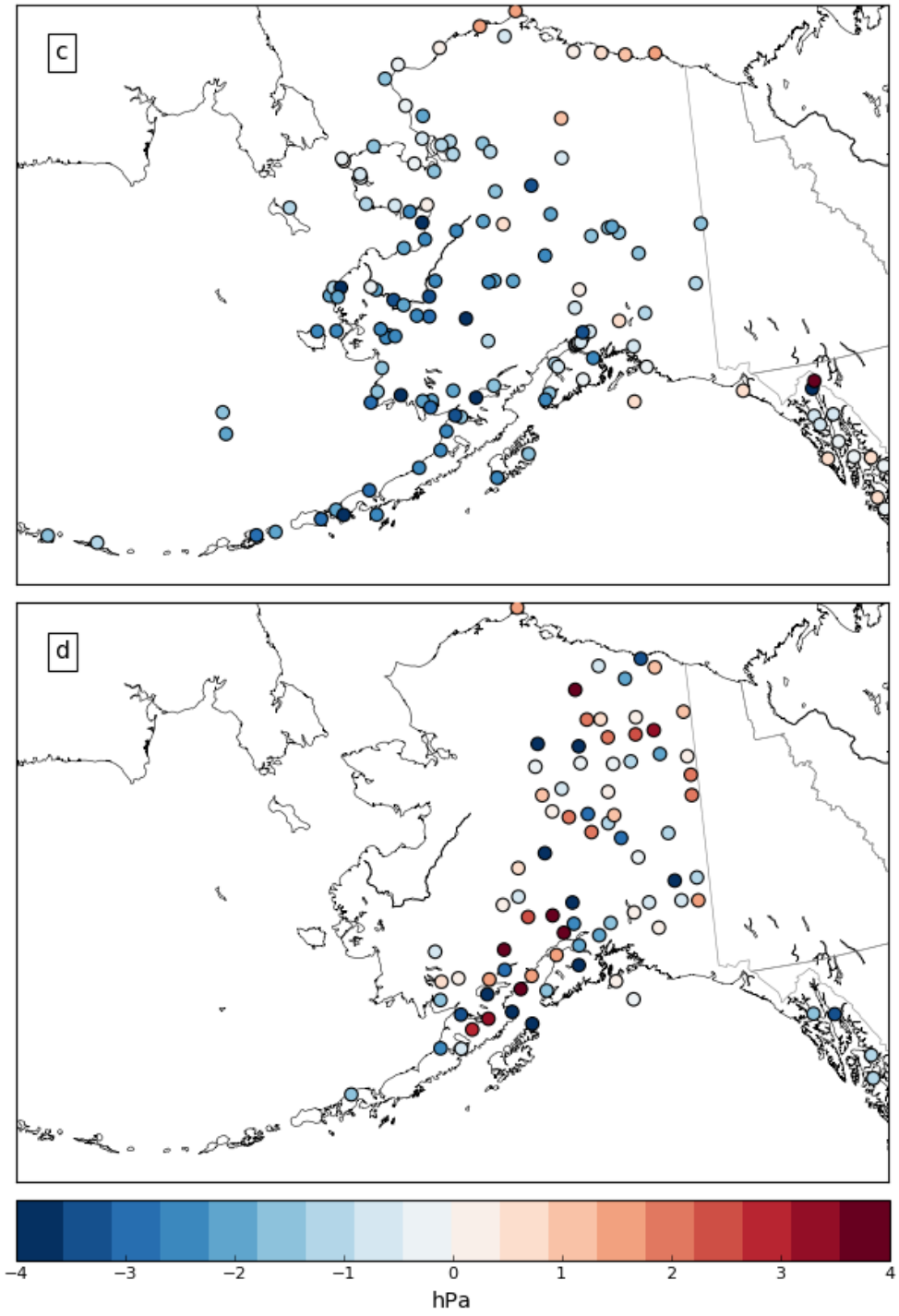

Figure 3.1 Continued.

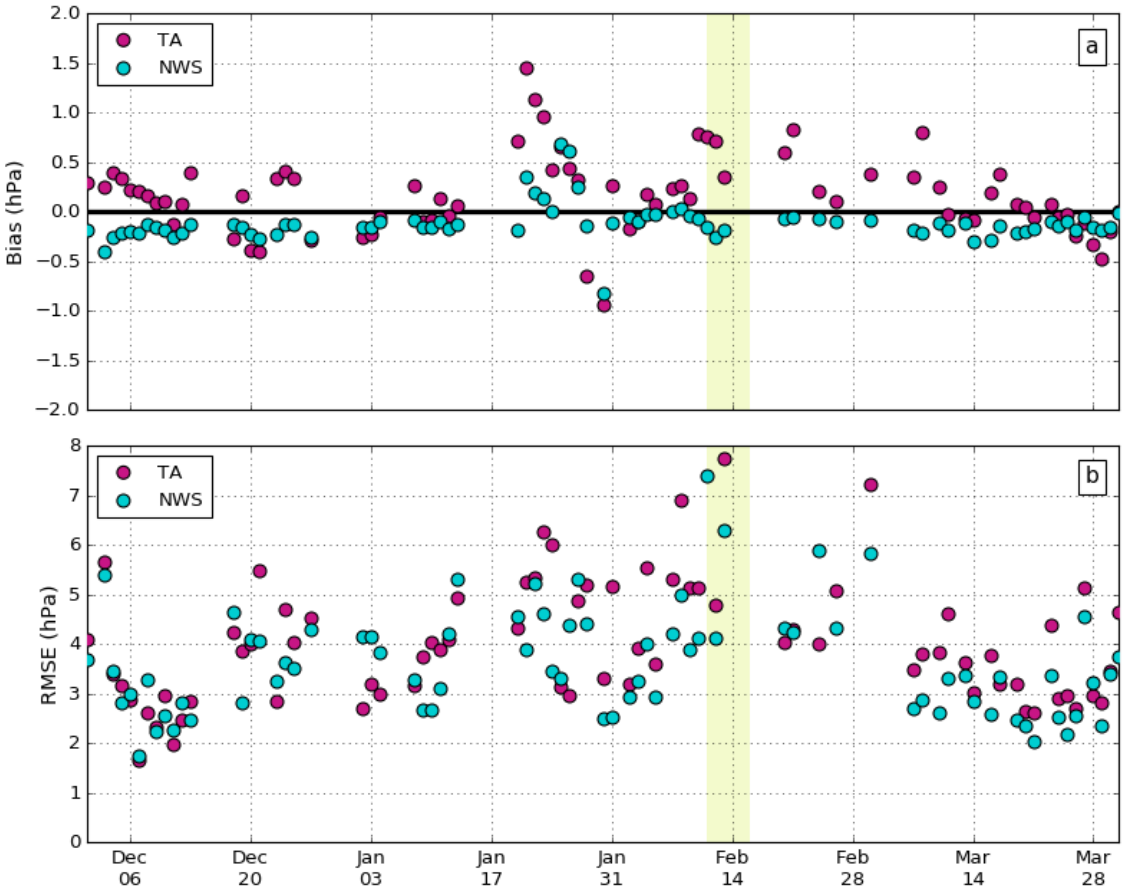

Figure 3.2. Average HRRR-AK altimeter setting statistics at each 00 UTC analysis time calculated relative to the corresponding altimeter setting values from the TA (magenta) and NWS (blue) networks. Statistical values include (a) average initial bias (hPa) of HRRR-AK analyses and (b) average RMSE (hPa) of the HRRR-AK altimeter setting 36-hour forecasts with the initial bias shown in (a) removed. The yellow shaded area highlights the case study period discussed in section 3.2.

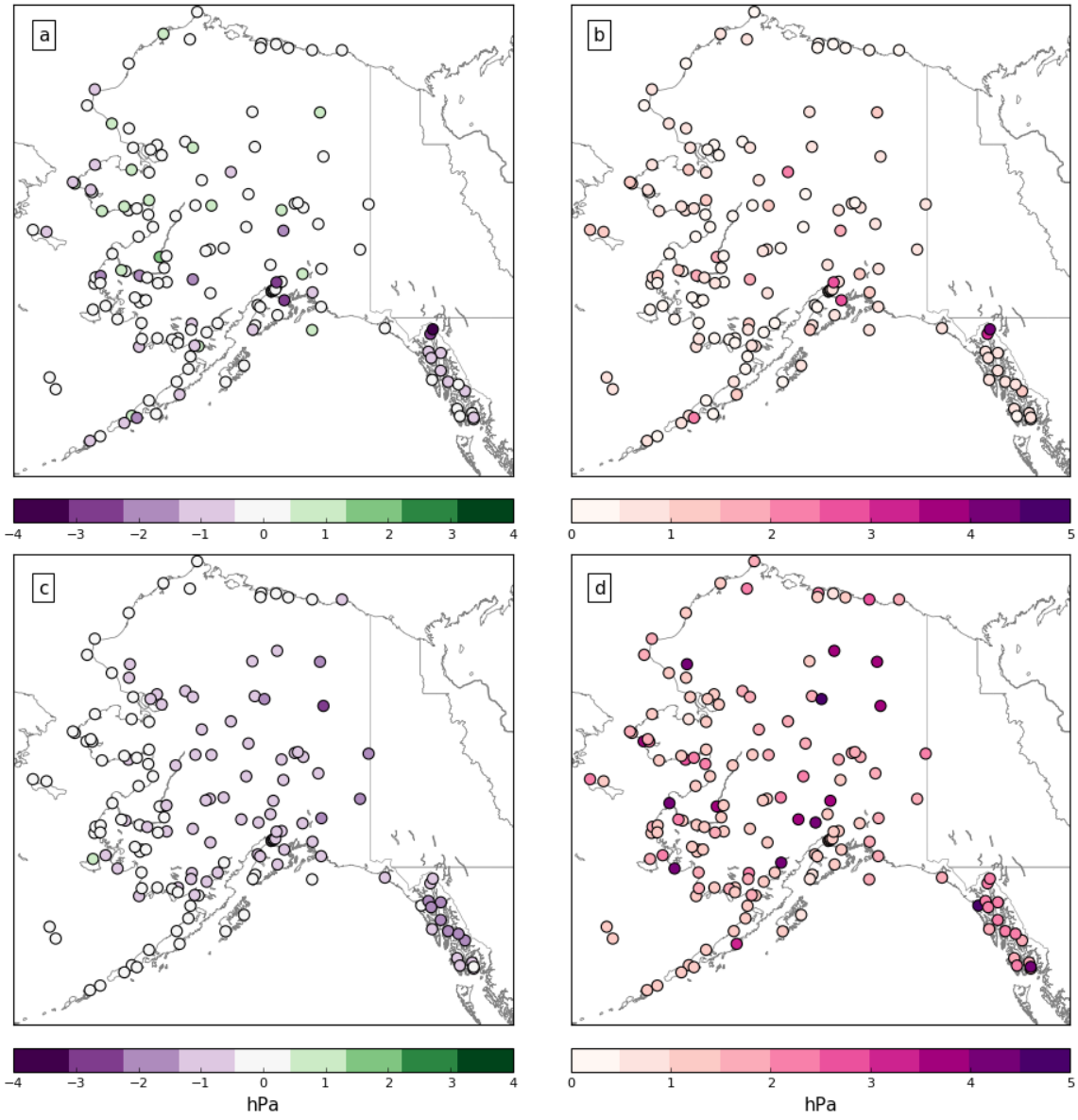

Figure 3.3. Winter 2017 HRRR-AK performance statistics. (a) Average initial bias (hPa, shaded according to the scale at the bottom) derived from all available 00 and 12 UTC HRRR-AK altimeter setting analyses relative to corresponding observations from NWS stations. (b) As in (a) except for Winter 2017 average initial RMSE. (c) As in (a) except for 36-hour forecasts with the initial bias removed. (d) As in (b) except for 36-hour forecasts with the initial bias removed.

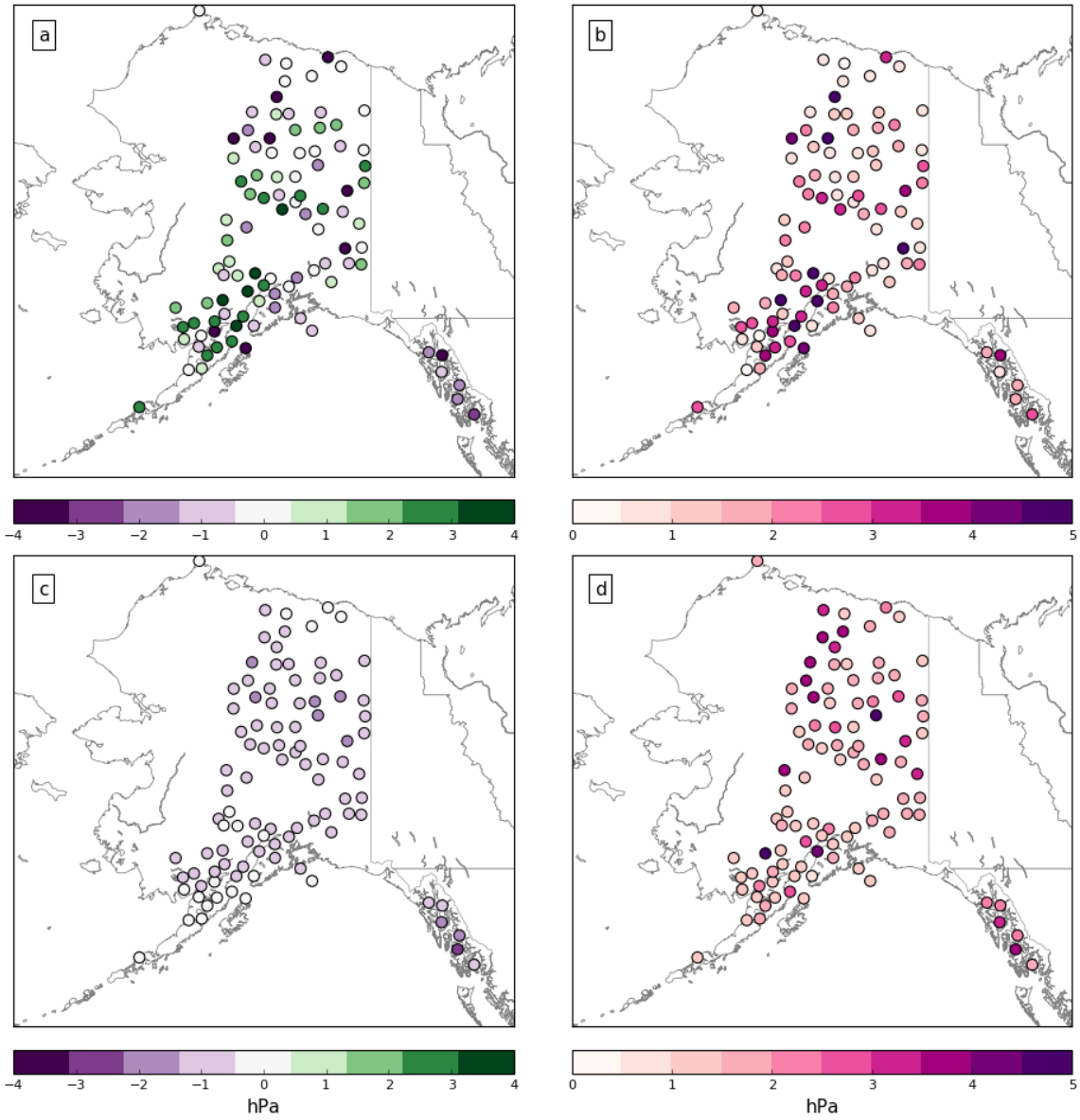

Figure 3.4. Winter 2017 HRRR-AK performance statistics. (a) Average initial bias (hPa, shaded according to the scale at the bottom) derived from all available 00 and 12 UTC HRRR-AK altimeter setting analyses relative to corresponding observations from TA stations. (b) As in (a) except for Winter 2017 average initial RMSE. (c) As in (a) except for 36-hour forecasts with the initial bias removed. (d) As in (b) except for 36-hour forecasts with the initial bias removed.

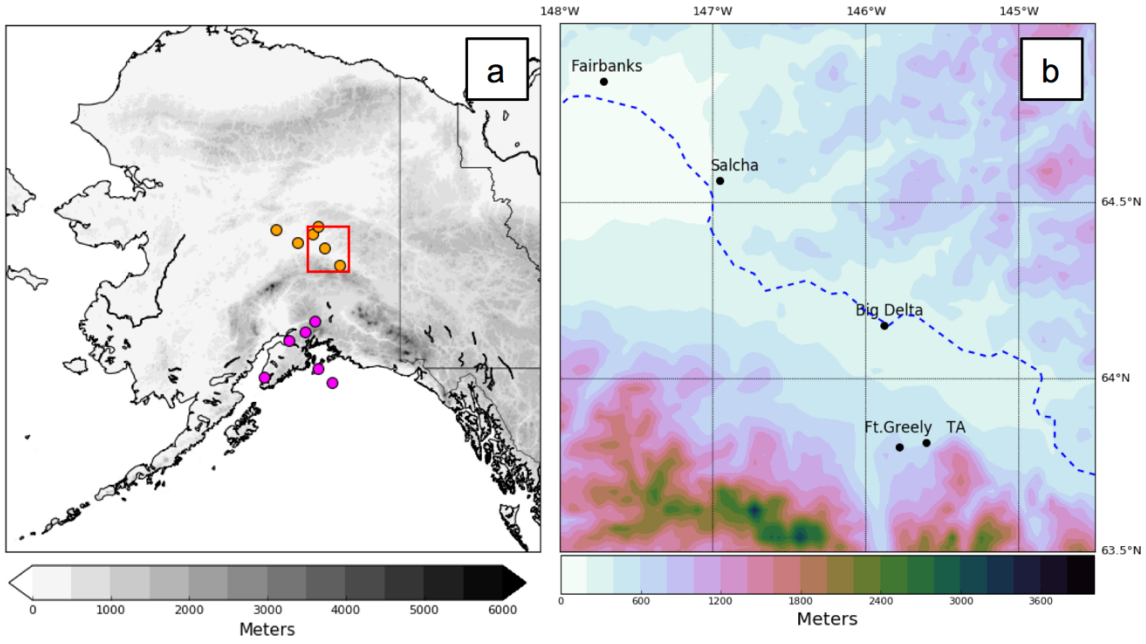

Figure 3.5. Alaska regions of interest for this thesis are shown. (a) Fairbanks – Tanana Valley stations (orange) and Anchorage – Gulf of Alaska stations (magenta) used in Figure 3.6. HRRR-AK surface elevation (m) is shaded in gray according to the scale at the bottom. (b) The region of interest for the 12-14 February 20127 case study delineated by the red box in (a). The blue dotted line denotes the Tanana River and weather conditions during the case study are examined at points labeled Fort Greeley (Station ID: TCOA2) and TA (Station ID: K24K).

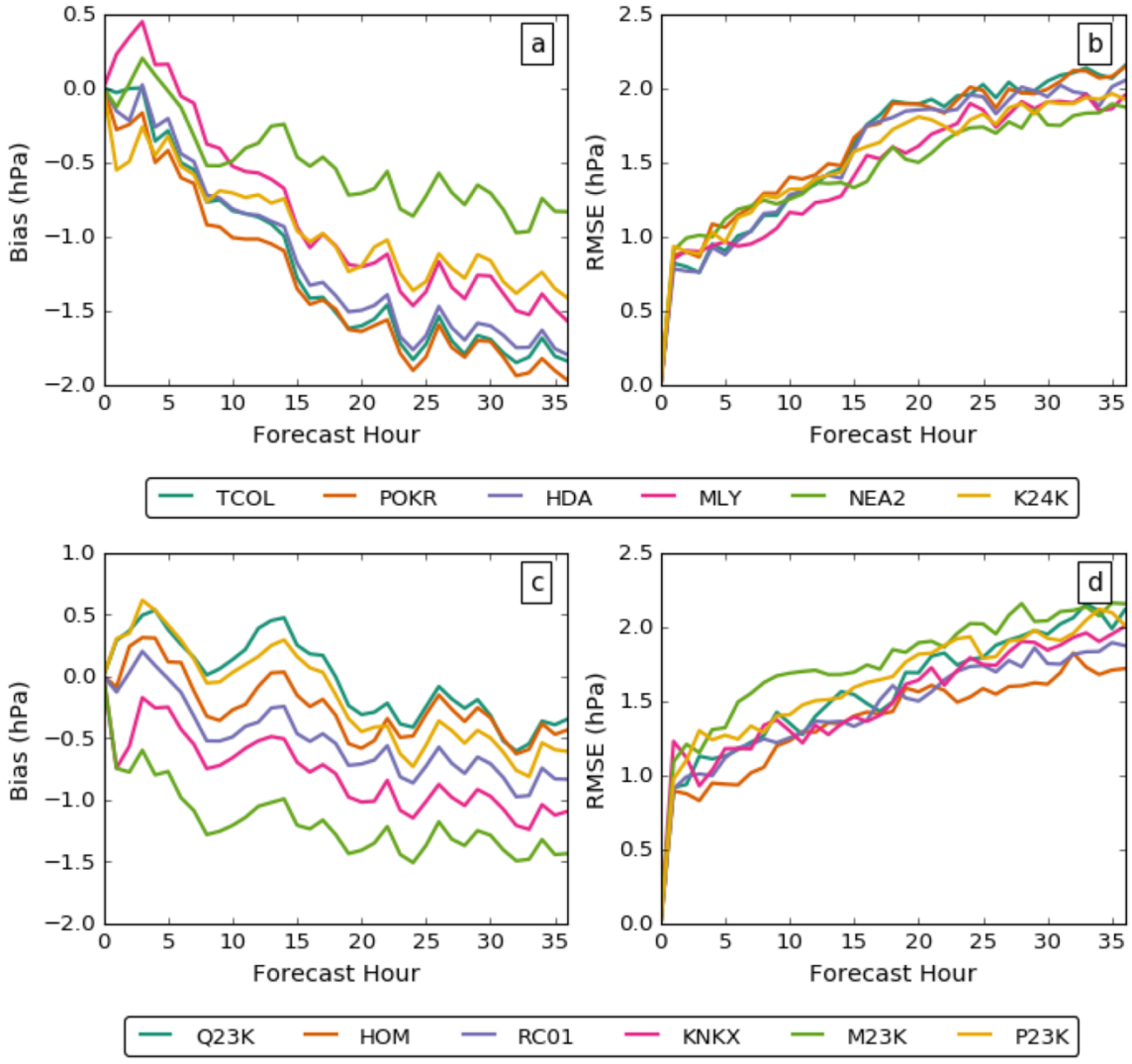

Figure 3.6. Winter 2017 average statistics computed for 0- to 36-hour forecasts derived from all available complete 00 and 12 UTC HRRR-AK model runs relative to corresponding observations from the 6 TA stations in the Fairbanks – Tanana Valley and Anchorage – Gulf of Alaska regions shown in Figure 3.5. (a) Average bias relative to the Fairbanks – Tanana Valley stations. (b) As in (a) except for average RMSE. (c) Average bias relative to the Anchorage – Gulf of Alaska stations. (d) As in (c) except for average RMSE.

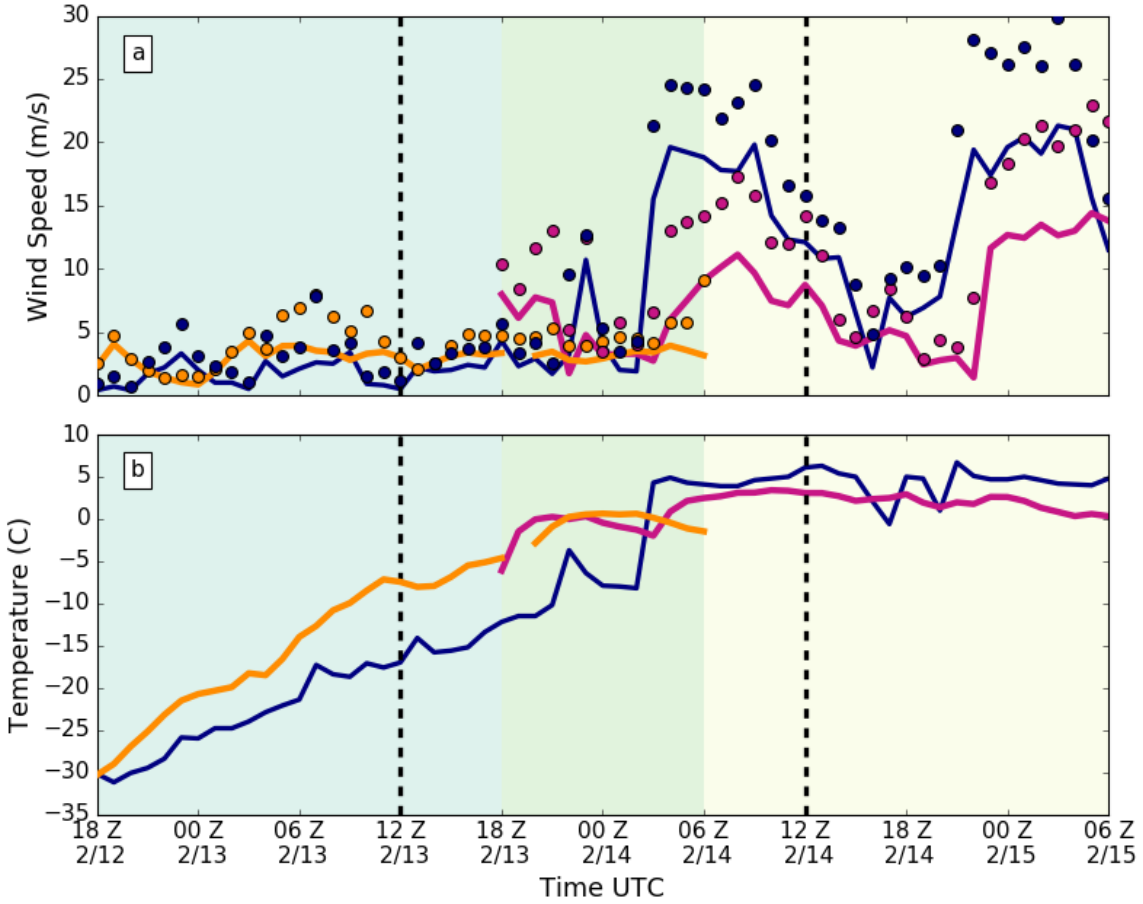

Figure 3.7. Time series of TCOA2 observations (navy) and nearest HRRR-AK grid point forecasts initialized on 18 UTC forecasts 12 February (orange) and 13 February (magenta) for (a) wind speed (m s^{-1}) and corresponding wind gusts (m s^{-1}) denoted by solid lines and dots, respectively, and (b) 2 meter temperature (°C). The black dashed lines at 12 UTC on 13 February and 14 February represent the times for which there is corresponding NUCAPS data.

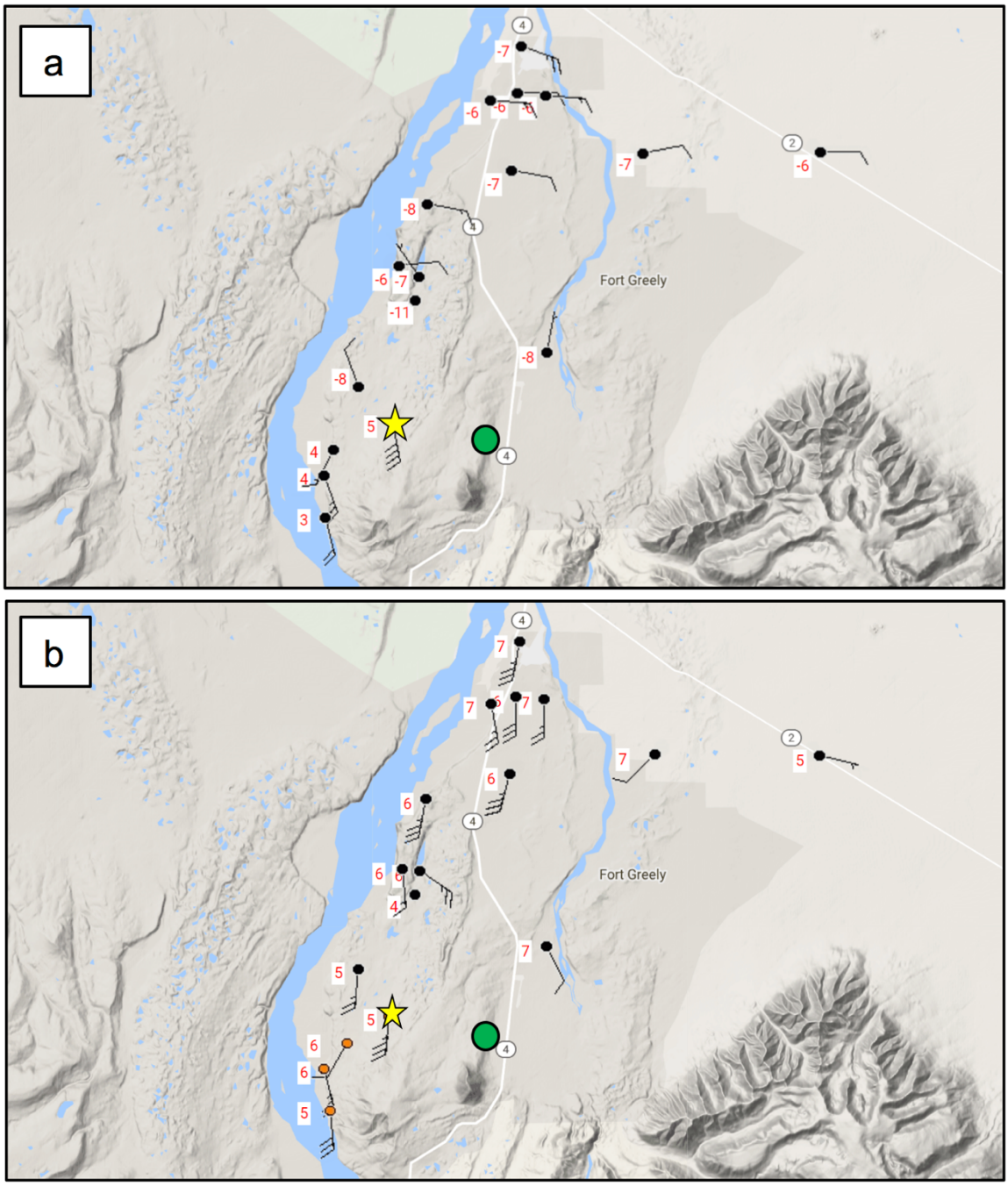

Figure 3.8. MesoWest observations of 10 m wind speed and direction (m s^{-1}) and 2 m temperature (°C; red numbers) from: (a) 03 UTC 14 February and (b) 00 UTC 15 February. Case study stations are marked by the yellow star (TCOA2) and the green circle (K24KX). Half, full, and flag wind barbs represent 2.5, 5, and 25 m s^{-1}, respectively.

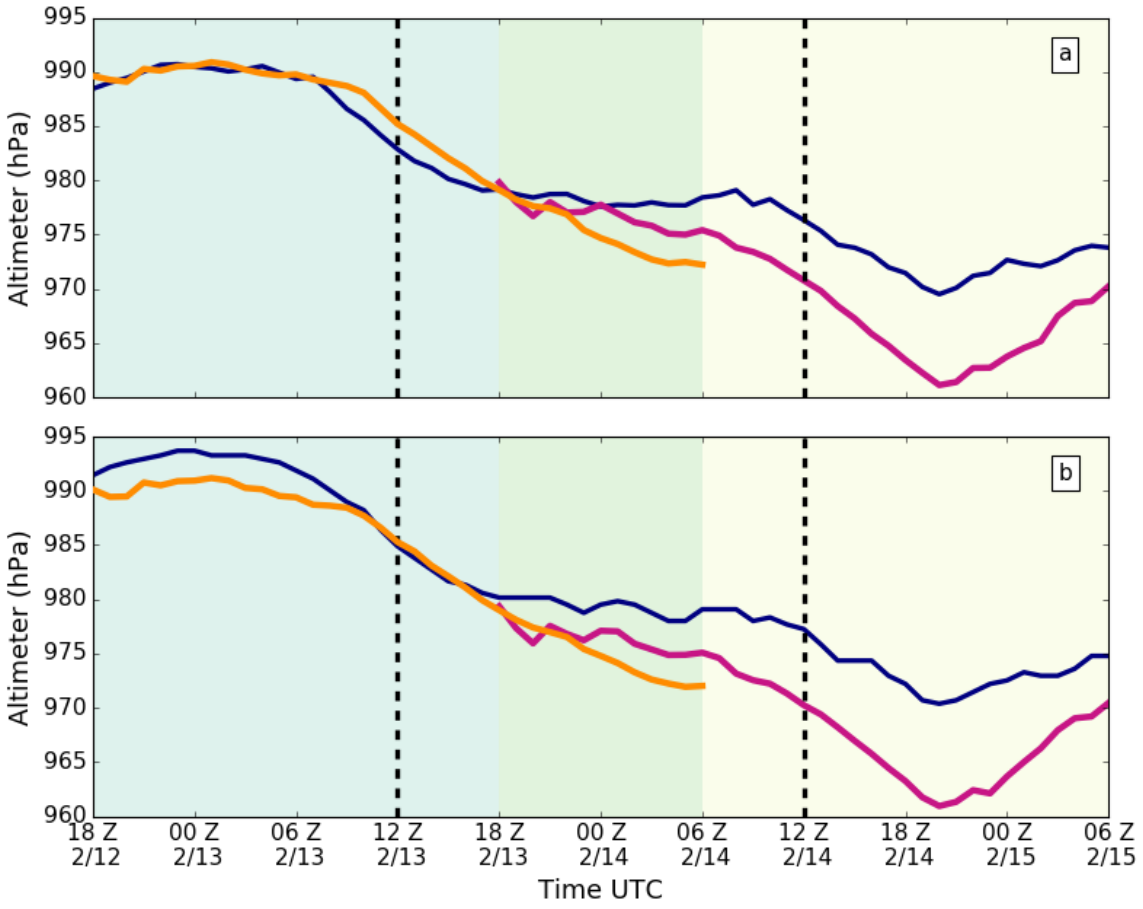

Figure 3.9. Time series of station observations (navy) compared with HRRR-AK forecasts initialized at 18 UTC 12 February (orange) and 18 UTC 13 February (magenta) from the model grid point nearest to (a) TCOA2 and (b) K24KX. Both station locations are noted again in Figure 3.8. The black dashed lines at 12 UTC on 13 February and 14 February represent the times for which there is corresponding NUCAPS data.

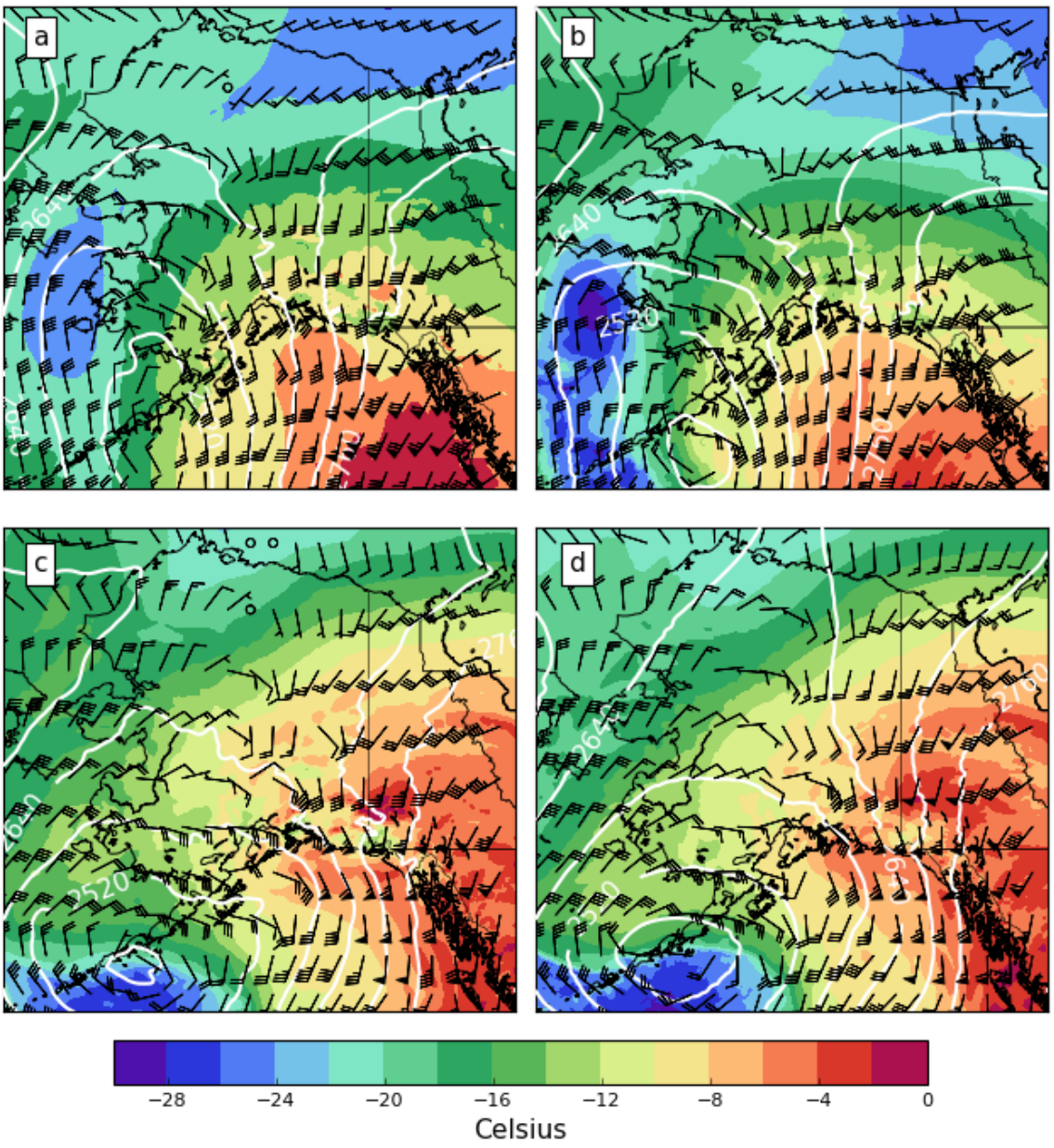

Figure 3.10. Temperature (shaded according to the scale at the bottom), heights (white contours at 60 m intervals), and wind vectors for: (a) 12 UTC 13 February HRRR-AK analysis, (b) 18-hour HRRR-AK forecast valid at 12 UTC 13 February, (c) 12 UTC 14 February HRRR-AK analysis, and (d) 18-hour HRRR-AK forecast valid at 12 UTC 14 February. Half, full, and flag wind barbs represent 5, 10, and 25 m s^{-1}, respectively.

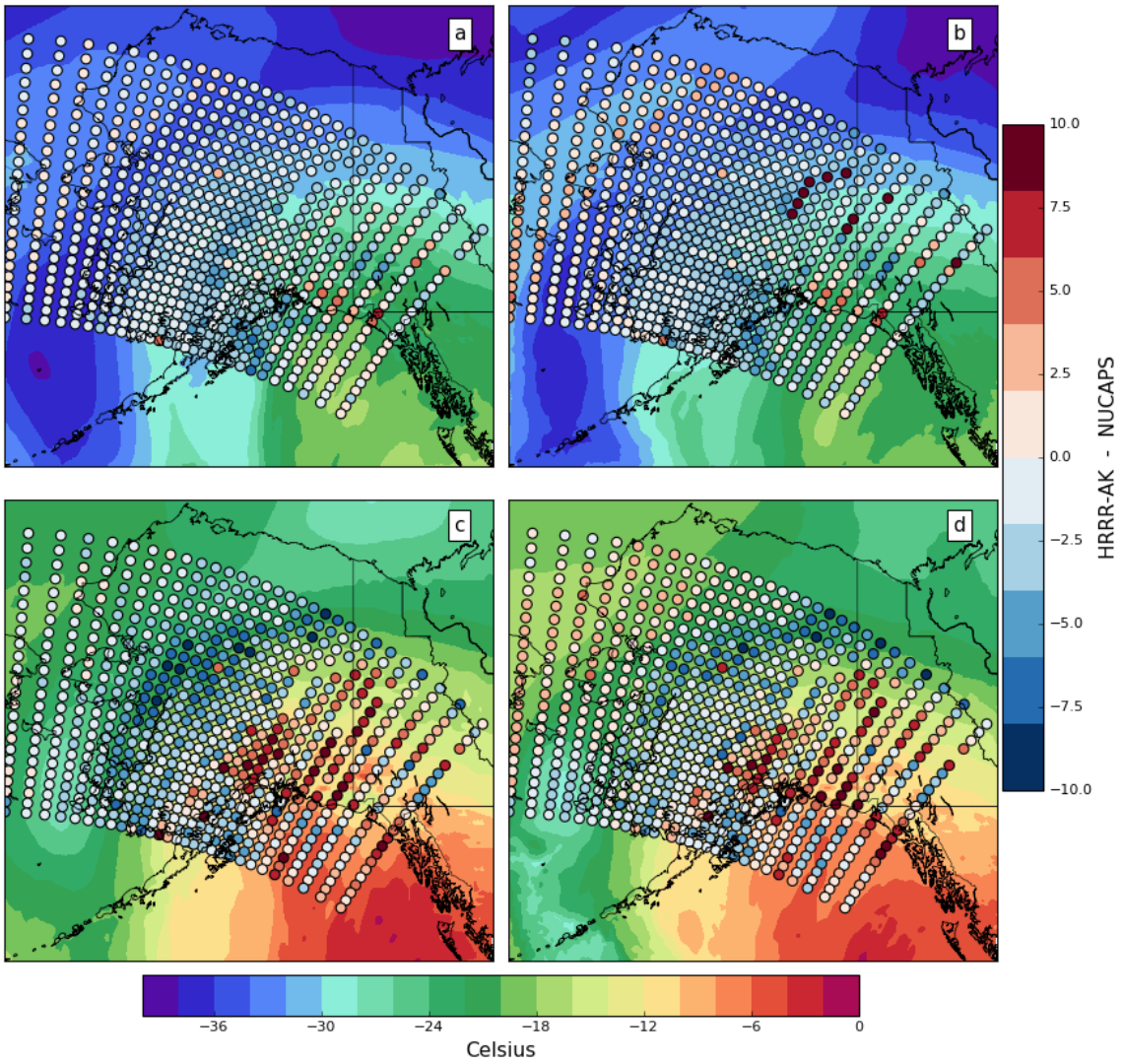

Figure 3.11. HRRR-AK 500 mb temperature forecasts validated with NUCAPS-derived products. (a) 12 UTC 13 February HRRR-AK 500 hPa temperature analysis (°C; shaded according to the scale at the bottom) and model bias with respect to the 500 hPa NUCAPS temperature data (°C; circles shaded according to the scale on the right), (b) 18-hour forecast of 500 hPa temperature (°C; shaded according to the scale on the bottom) and model bias with respect to the 500 hPa NUCAPS temperature data (°C; circles shaded according to the scale on the right), (c) same as (a) but for 700 hPa, (d) same as (b) but for 700 hPa.

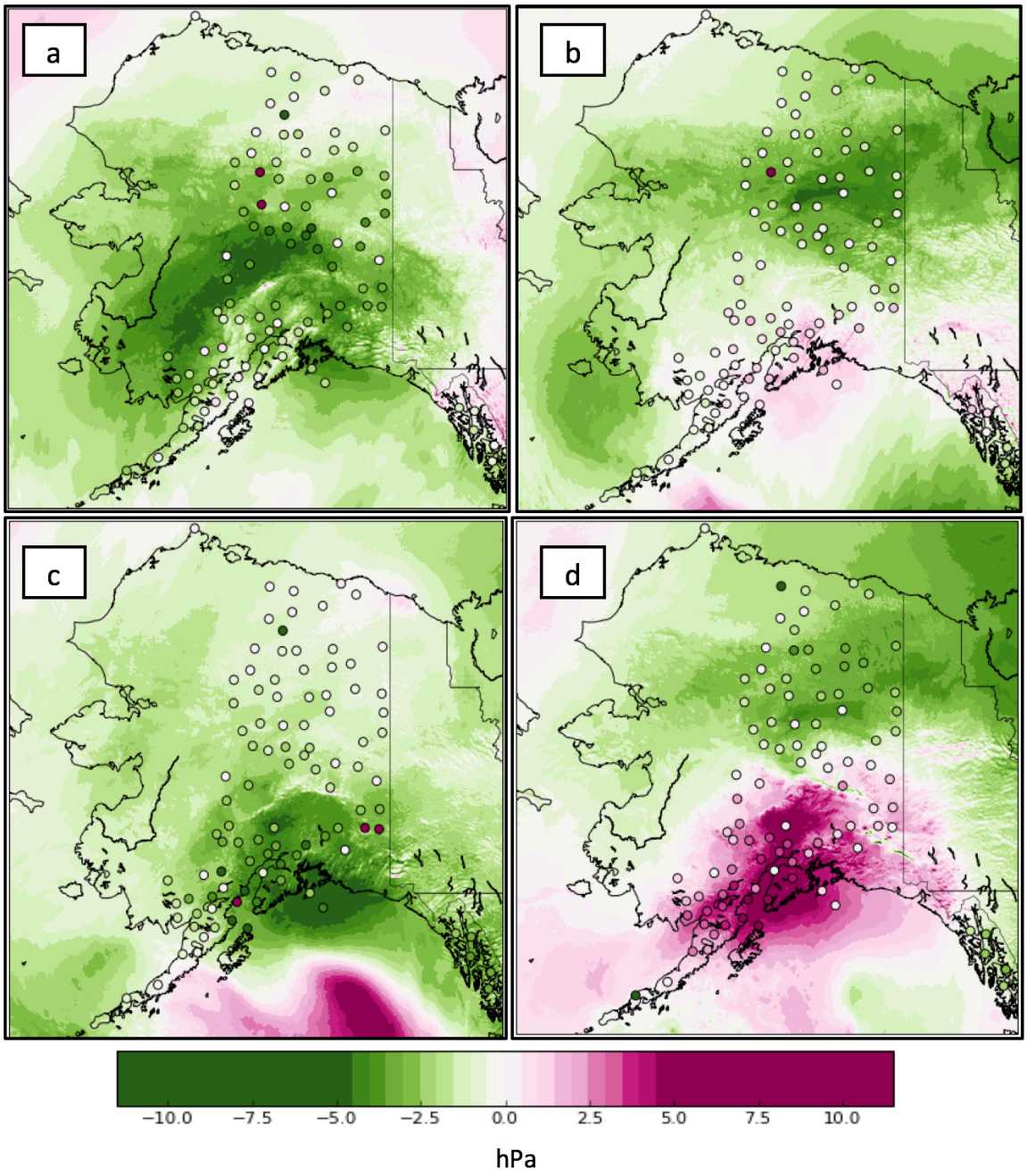

Figure 3.12. The 3-hour forecast tendency of the HRRR-AK altimeter setting (hPa, shaded according to the scale at the bottom) and 3-hour tendency of the altimeter setting (hPa, shaded circles) observed by the TA stations for the corresponding valid times for: (a) 12-hour forecast valid at 12 UTC 13 February, b) 24-hour forecast valid at 00 UTC 14 February, (c) 12-hour forecast valid at 12 UTC 14 February, d) 24-hour forecast valid at 00 UTC 15 February.

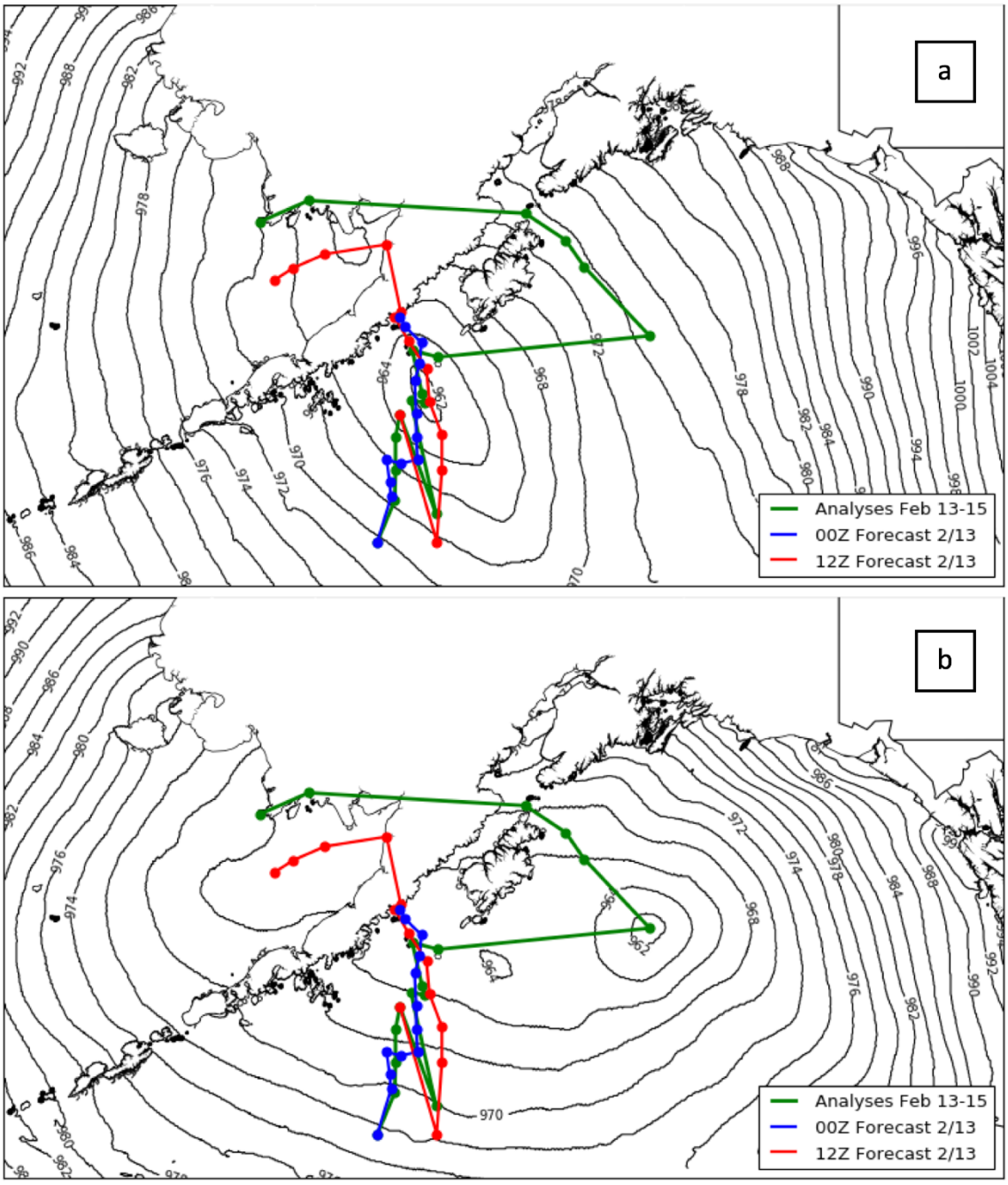

Figure 3.13. Altimeter setting (hPa, contoured at 2 hPa intervals) valid at: (a) 00 UTC 14 February 2017 and (b) 09 UTC 14 February 2017. Duplicated in both panels are the locations of the center of lowest pressure at 3-hour intervals using HRRR-AK analyses (green) and forecasts from the HRRR-AK model runs initialized at 00 UTC 13 February (blue) and 12 UTC 13 February 12 UTC (red).

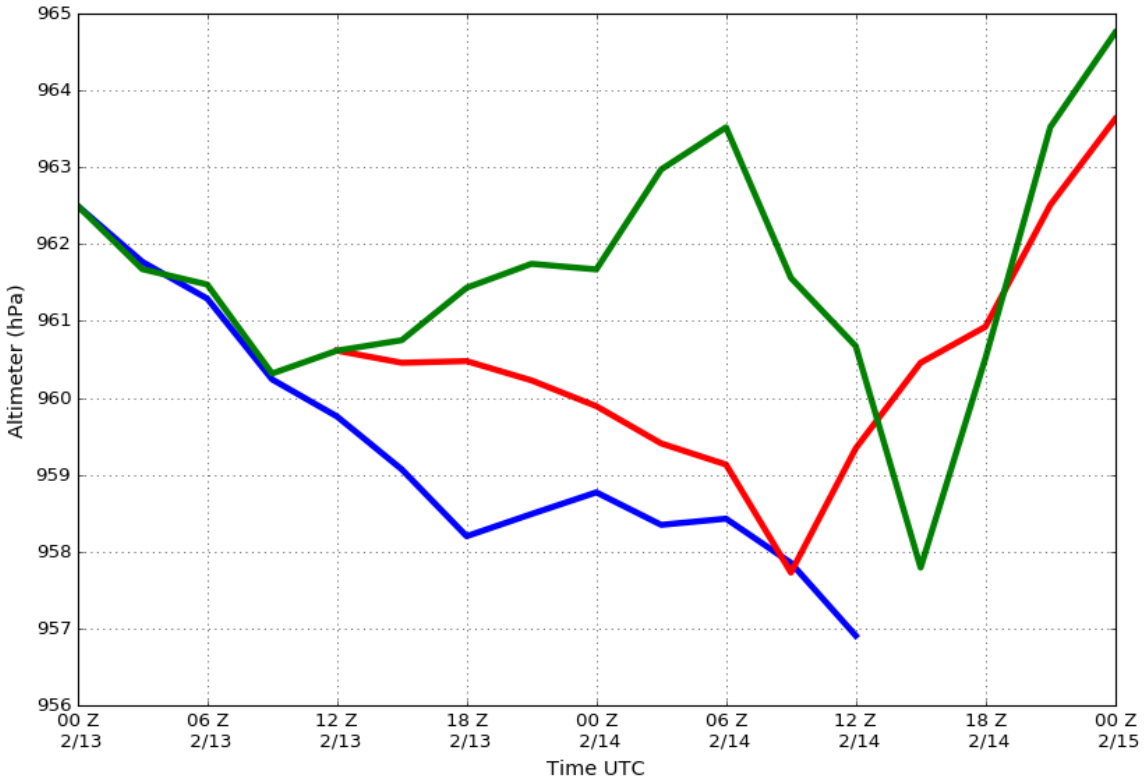

Figure 3.14. Magnitude of the center of lowest altimeter setting (hPa) corresponding to the tracks shown in Figure 3.9 from HRRR-AK analyses (green) and forecasts from the HRRR-AK model run initialized at 00 UTC 13 February (blue) and 12 UTC 13 February 12 UTC (red).

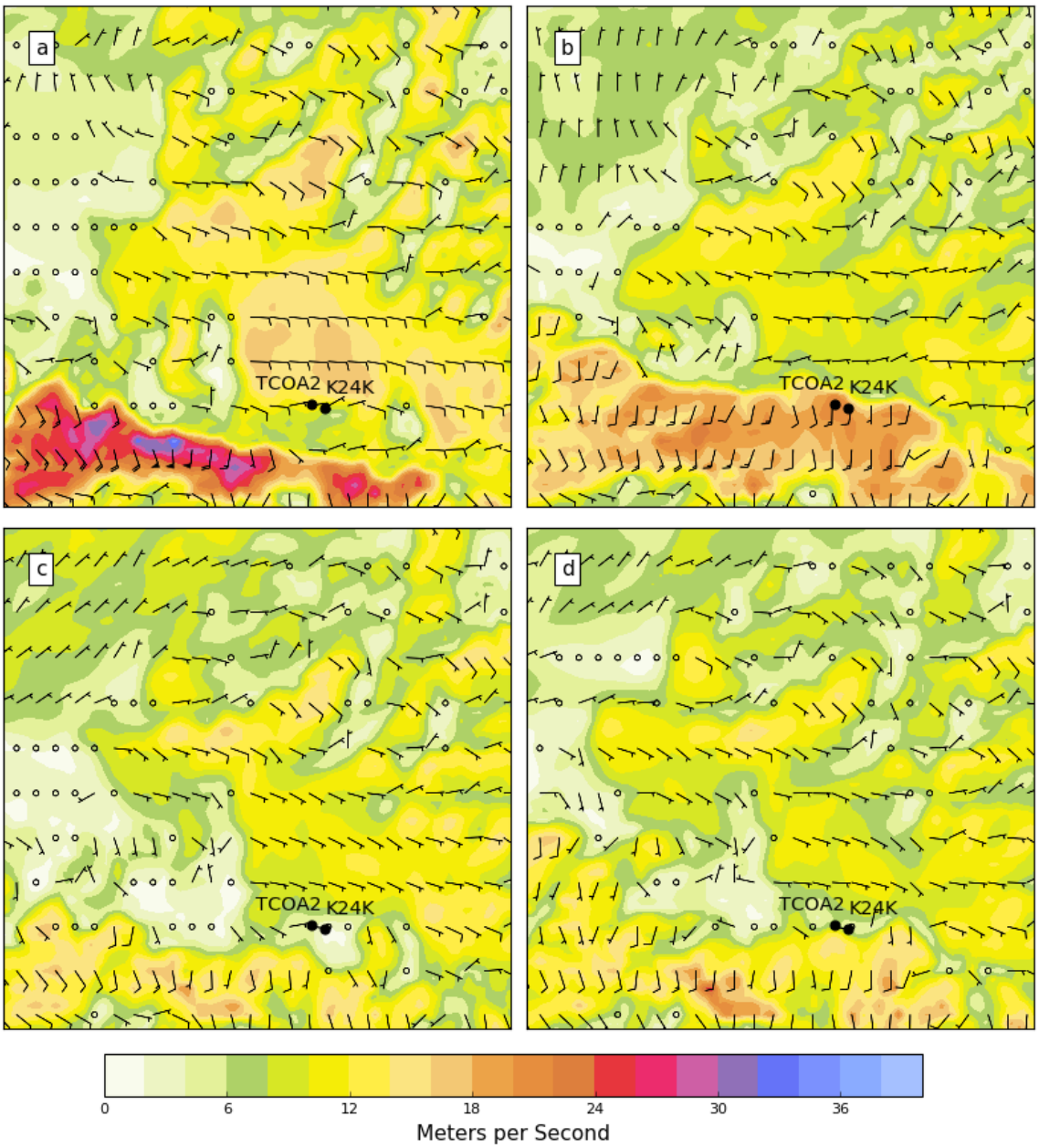

Figure 3.15. HRRR-AK 10 m wind vectors (m s^{-1}) and wind gust contours (m s^{-1}; shaded according the scale below) valid for: (a) 12 UTC analysis on 13 February, (b) 03 UTC analysis on 14 February, (c) 33-hour forecast valid at 03 UTC 14 February, and (d) 9-hour forecast valid at 03 UTC 14 February. Half, full, and flag wind barbs represent 5, 10, and 25 m s^{-1}, respectively.

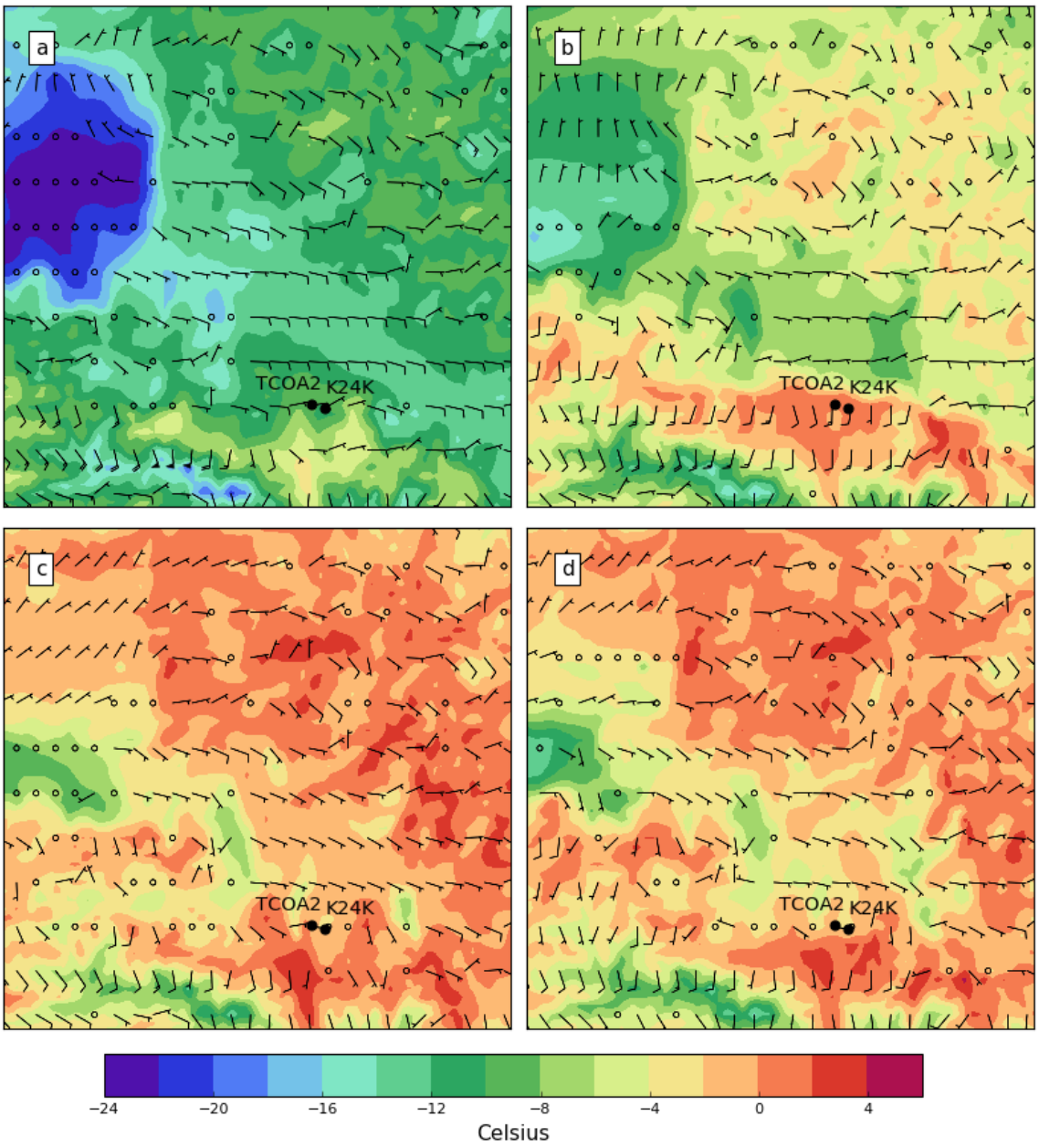

Figure 3.16. HRRR-AK 10 m wind vectors (m s^{-1}) and 2 m temperature contours (°C; shaded according the scale below) valid for: (a) 12 UTC analysis on 13 February, (b) 03 UTC analysis on 14 February, (c) 33-hour forecast valid at 03 UTC 14 February, and (d) 9-hour forecast valid at 03 UTC 14 February. Half, full, and flag wind barbs represent 5, 10, and 25 m s^{-1}, respectively.

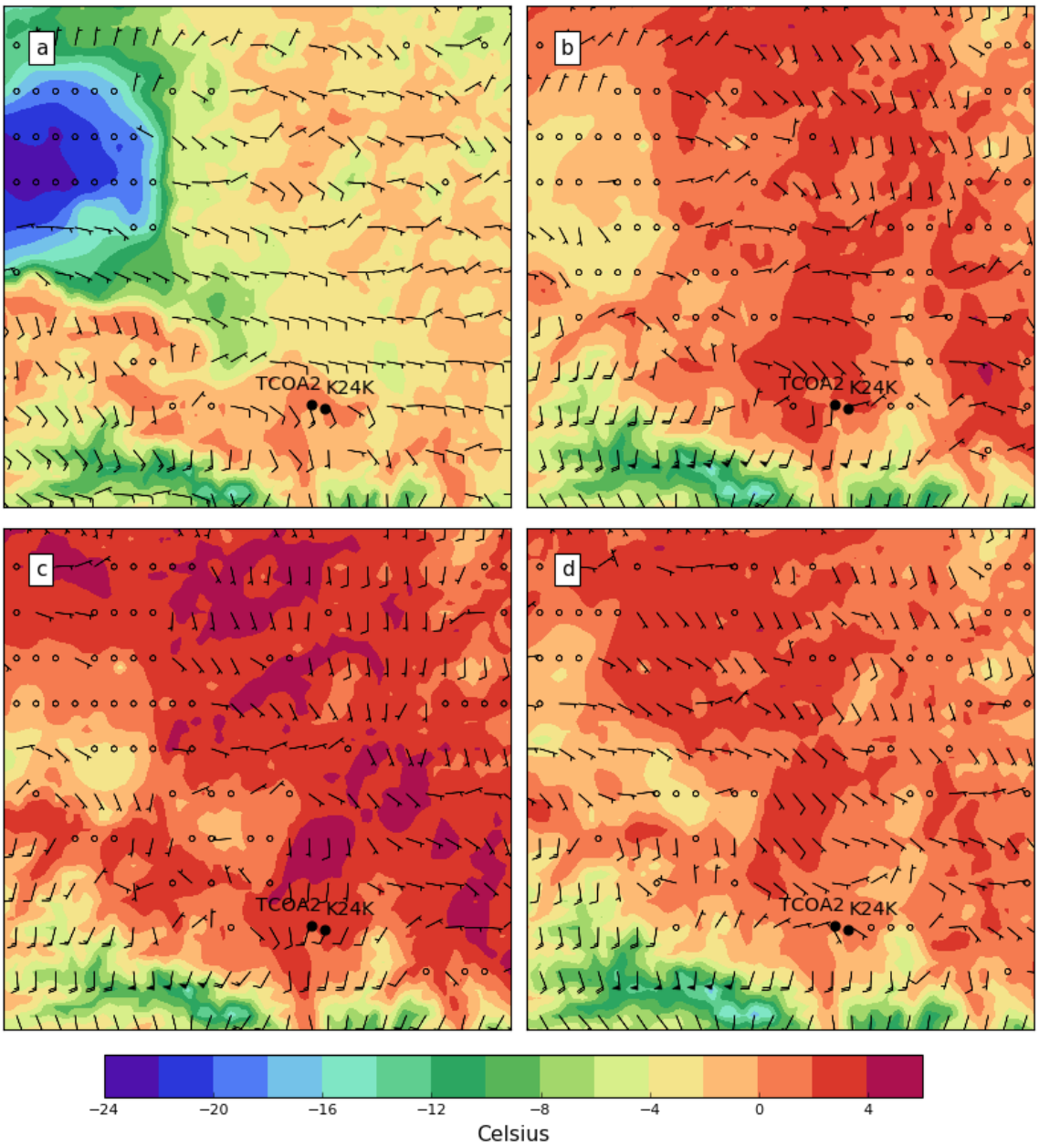

Figure 3.17. HRRR-AK 10 m wind vectors (m s^{-1}) and 2 m temperature contours (°C; shaded according the scale below) valid for: (a) 12 UTC analysis on 14 February, (b) 00 UTC analysis on 14 February, (c) 30-hour forecast valid at 00 UTC 15 February, and (d) 6-hour forecast valid at 00 UTC 15 February. Half, full, and flag wind barbs represent 5, 10, and 25 m s^{-1}, respectively.

CHAPTER 4

CONCLUSION

4.1 Summary

Over the course of the 2017 winter, the experimental HRRR-AK analyses and forecasts were evaluated using altimeter setting data from the TA and the NWS networks across Alaska. The HRRR modeling system for Alaska has been under development over the past several years. After a major upgrade in late November 2016 that included changing the forecast domain, the stability of the model's configuration and improved availability of the analysis and forecast grids from ESRL provided the opportunity to undertake this study for the 2017 winter season. With the model intended to become operational in early 2018, this research helps provide useful guidance on some of the characteristics of the modeling system's performance.

The original intent of this study was to investigate the HRRR-AK's ability to forecast the phasing and progression within a small sample of major winter storms, particularly along the Aleutian Low storm track. However, the 2017 winter was comparatively quiescent in regards to large-scale storms traversing in the vicinity of the Aleutians. Large-scale circulation features that influence Alaska's regional weather patterns such as the AO and PNA were positive and negatively phased, respectively, for the bulk of the season, contributing to an anomalously weak Aleutian storm track. Thus,

the goals of the research shifted to performing aggregate statistics of the model's ability to forecast surface pressure reduced to altimeter setting as well as to investigate a case study in mid-February when the average model skill coincidentally reached a seasonal low and during which strong downslope winds were observed in the upper reaches of the Tanana Valley near Fort Greely. While other variables are examined during the case study, the primary variable for validation of the HRRR-AK model is surface pressure reduced to the altimeter setting. Surface pressure was chosen as the primary metric for determining model skill due to its higher degree of reliability over spatial scales, on the order of tens of km, than other more location-sensitive variables. In addition, surface pressure was chosen in order to include the USArray TA network and as many other data resources as possible to evaluate the HRRR-AK.

Skill of the HRRR-AK was quantified by calculating aggregate statistics with surface data from the in-situ TA and NWS networks. NUCAPS-derived temperature profiles were examined as an attempt to evaluate the mid-tropospheric conditions during the 12-15 February period. The only comparison that proved to be useful was at the 500 hPa level, as the bias and RMSE between the model analyses and forecasts and NUCAPS data grew increasingly large in the lower troposphere, indicating errors in the NUCAPS temperatures rather than in the HRRR-AK products. The NUCAPS-derived data products and other datasets from polar-orbiting satellites are currently being validated with respect to the HRRR-AK at NOAA ESRL and the University of Alaska – Fairbanks for possible use in the model's assimilation procedures (Lin et al. 2017). Assimilating satellite radiance data directly is generally found to be preferable to assimilating derived products such as the NUCAPS temperature.

The TA pressure data proved to be very useful to evaluate the accuracy of the HRRR-AK analyses and forecasts. The TA was originally deployed as a seismic monitoring network, but through the addition of pressure sensors and Vaisala all-in-one meteorological sensors, it has become an invaluable asset for weather observation, research and forecasting, especially in data sparse Alaska. The research quality TA not only produces high temporal resolution pressure data, but the metadata for the station siting is very precise, especially compared to other networks. This fact alone is crucial for this model evaluation as the reduction of surface pressure to altimeter setting relies on the station's elevation, and is extrapolated down to sea level. Since observations from the TA are currently not assimilated in the HRRR-AK, this created an opportunity to evaluate model output with an in-situ dataset that is being assimilated (NWS) and one that is not (TA). The inter-comparison of these datasets with model analyses revealed its dependency on the relatively small number of assimilated in-situ pressure observations with larger initial discrepancies with the unassimilated data.

The use of the TA and NWS networks for model verification allowed for the skill of the HRRR-AK to be evaluated in a number of ways throughout the 2017 winter. Since reduction to altimeter setting is an imperfect approximation of sea level pressure given the assumed standard atmosphere profile below ground, individual hourly or seasonally-averaged maps of altimeter setting exhibit erroneously low values over regions of higher terrain. This limitation was mitigated by removing the difference in altimeter setting between the HRRR-AK analyses and the observations from the subsequent differences between the forecasts in the same model run and the observations at the corresponding valid times.

The aggregate winter 2017 statistics concerning the skill of the model's altimeter setting forecasts were computed spatially and temporally, for all stations in both the NWS and TA networks. The altimeter setting biases for the TA stations at the time of the 00 and 12 UTC HRRR-AK analyses (initial biases) were much larger than the biases for the NWS stations. The average initial biases for the TA network were larger in magnitude than the average initial bias for the NWS network for analyses initialized at either 00 or 12 UTC throughout the duration of the winter. This was also true spatially, when the average initial bias was calculated at each individual TA station for all 00 and 12 UTC analyses with complete forecasts, returning much larger initial bias values than for most NWS stations. Once the initial biases were removed, the average RMSE's for the 00 UTC 36-hour forecasts were nearly identical for both the TA and NWS throughout the 2017 winter season, with the worst model skill of the season for both networks occurring during the period of the case study. These results were mirrored spatially when the initial bias was removed from each station; the average 36-hour bias and RMSE at each TA station were consistent with the values at the NWS stations, exhibiting the model's loss of mass at station locations from both networks by the end of the forecast cycle. The forecast hour-to-hour evolution of bias and RMSE were illustrated for two subdomains: the Fairbanks – Tanana Valley and Anchorage – Gulf of Alaska regions. The RMSEs in the Tanana Valley appeared to be dominated by the downward negative trend in the difference between model forecasts and observations common throughout much of the model domain while the errors for the Anchorage stations may be more affected as well by the model's skill in handling travelling weather disturbances.

With regards to the case study period, the HRRR-AK analyses were very useful

for diagnosing the spatial and temporal evolution of the prevailing conditions aloft and sensible weather near the surface associated with the progression of the cut-off low in the Gulf of Alaska and subsequent development of two distinct periods of downslope winds in the Fort Greely area of the Tanana Valley. As indicated in the aggregate pressure skill metrics, HRRR-AK forecast accuracy was lower during this period than at other times during the winter. Overall, the forecast accuracy at lead times of 18- to 36-hours for the synoptic-scale conditions in the Alaska region were generally adequate. However, errors in the details regarding the intensity and position of small features embedded within the cut-off low may have led to excessive deepening of the surface low and downstream mid-tropospheric warm air advection that affected the accuracy of the local forecasts in the Fort Greely area. Temperature, wind speed, and pressure errors at 18- to 36-hour lead times of 10°C, 10 m s^{-1}, and 10 hPa, respectively, were noted locally.

4.2 Future Work

The benefits of the USArray will continue to be felt in the state of the Alaska with the ongoing deployment of the network throughout summer 2017. As of June 2017, additional stations have already been deployed in western Alaska, with more stations expected to be deployed in the northwest portion of the state later this summer (Figure 4.1). Once fully deployed, the ~200 TA stations will remain in Alaska until at least 2019, with the extension of the deployment contingent upon funding. There is high interest to maintain the network indefinitely by many weather-related Alaskan stakeholders.

The data obtained from the TA during summer 2017 will be utilized for additional evaluation of the HRRR-AK for the warm season. The analysis methods

outlined in Chapter 2 will be repeated for the months of June, July, and August 2017, which will produce a subsequent set of aggregate statistics to be compared to those calculated during winter 2017. Improved nowcasting and forecasting of the conditions impacting summer season wildfires is of considerable interest. A 2-year study to evaluate the accuracy of the HRRR-AK in the vicinity of major wildfires in the continental United States and Alaska will begin later this summer, which will be funded by a grant from the Joint Fire Science Program.

The HRRR-AK data assimilation procedures set to become operational in early 2018 are about to be transitioned from ESRL to NCEP and will not include observations from the TA or many other Alaska mesonet observations available via MesoWest. However, ESRL model developers are interested to examine the impact of these observations on the next experimental version of the HRRR-AK that will be available later this summer. While this study was not an exhaustive model evaluation, the results from this research can serve as a baseline to determine how the implementation of additional surface observations affects the accuracy of the altimeter setting forecasts produced by the model and aim to help improve Alaska's first hourly 3 km atmospheric model.

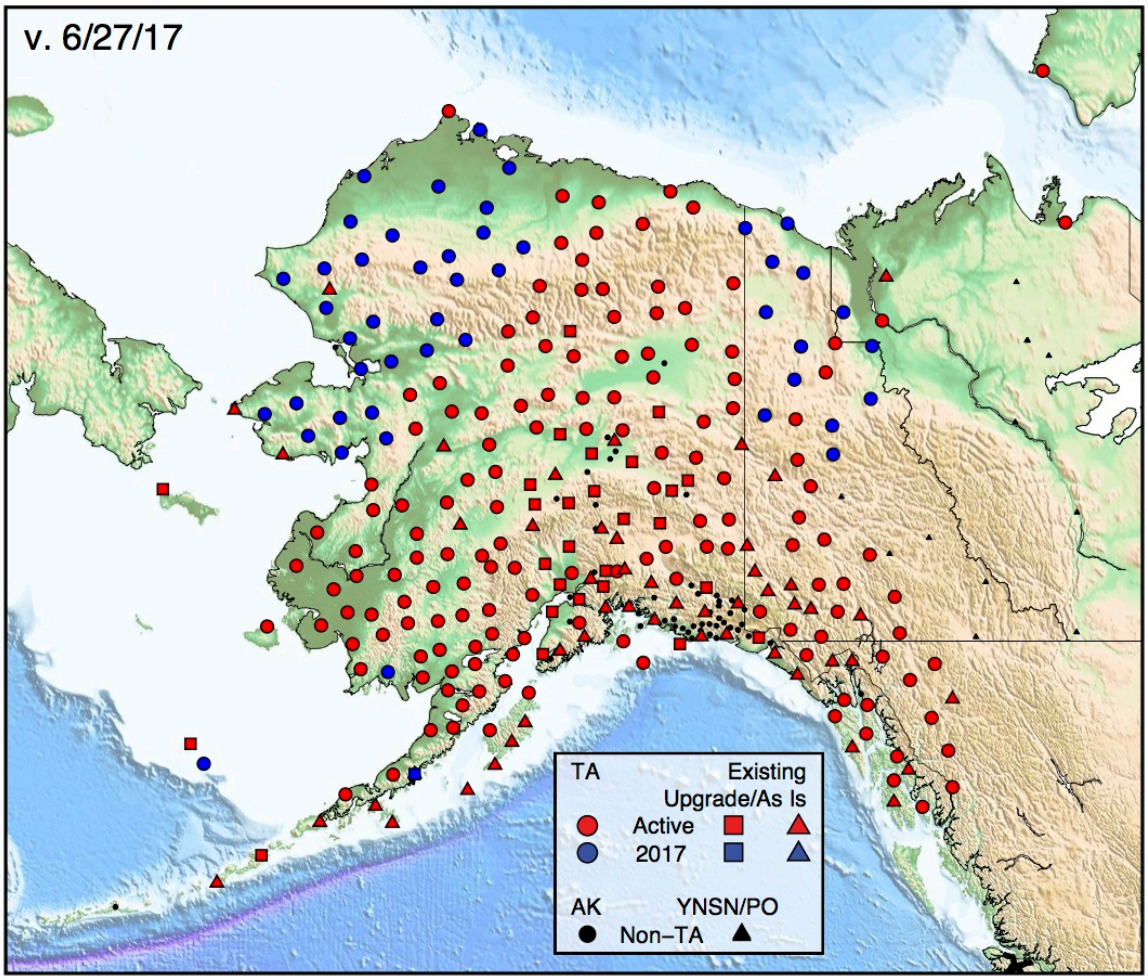

Figure 4.1. Valid on 27 June 2017, the current status of deployment of the USArray TA in the state of Alaska. The red symbols represent stations that are deployed and currently active. The blue symbols are planned station deployments during the summer of 2017.

REFERENCES

Ancell, B.C., 2012: Examination of Analysis and Forecast Errors of High-Resolution Assimilation, Bias Removal, and Digital Filter Initialization with an Ensemble Kalman Filter. *Mon. Wea. Rev.*, **140**, 3992–4004, doi: 10.1175/MWR-D-11-00319.1.

Benjamin, S. G., B. E. Schwartz, and R. E. Cole, 1999: Accuracy of ACARS Wind and Temperature Observations Determined by Collocation. *Wea. Forecasting*, **14**, 1032–1038, doi: 10.1175/1520-0434(1999)014<1032:AOAWAT>2.0.CO;2.

Benjamin, S. G., S. S. Weygandt, J. M. Brown, M. Hu, C. R. Alexander, T. G. Smirnova, J. B. Olson, E. P. James, D. C. Dowell, G. A. Grell, H. Lin, S. E. Peckham, T. L. Smith, W. R. Moninger, J. S. Kenyon, and G. S. Manikin, 2016: A North American Hourly Assimilation and Model Forecast Cycle: The Rapid Refresh. *Mon. Wea. Rev.*, **144**, 1669–1694, doi: 10.1175/MWR-D-15-0242.1.

Bieniek, P. A., U. S. Bhatt, L. A. Rundquist, S. D. Lindsey, and X. D. Zhang, 2011: Large-scale Climate Controls of Interior Alaska Ice Breakup. *J. Climate*, **24**, 286–297, doi:10.1175/2010JCLI3809.1.

Bieniek, P. A., U. S. Bhatt, R. L. Thoman, H. Angeloff, J. Partain, J. Papineau, F. Fritsch, E. Holloway, J. E. Walsh, C. Daly, M. Shulski, G. Hufford, D. F. Hill, S. Calos, and R. Gens, 2012: Climate Divisions for Alaska Based on Objective Methods. *J. Appl. Meteor. Climatol.*, **51,** 1276–1289, doi: 10.1175/JAMC-D-11-0168.1.

Bieniek, P. A., J. E. Walsh, R. L. Thoman, and U. S. Bhatt, 2014: Using Climate Divisions to Analyze Variations and Trends in Alaska Temperature and Precipitation. *J. Climate*, **27**, 2800–2818, doi: 10.1175/JCLI-D-13-00342.1.

Bienek, P. A., U. S. Bhatt, J. E. Walsh, T. S. Rupp, J. Zhang, J. R. Krieger, and R. Lader, 2016: Dynamical Downscaling of ERA-Interim Temperature and Precipitation for Alaska. *J. Appl. Meteor. Climatol.*, **55**, 635–654, doi: 10.1175/JAMC-D-15-0153.1.

Blaylock, B. K, J. Horel, S. Liston, 2017: Cloud Archiving and Data Mining of High Resolution Rapid Refresh Model Output. *Computers and Geoscieneces.* Submitted.

Bluestein, H. B., 1992: *Synoptic-Dynamic Meteorology in Midlatitudes. Vol I: Principles of Kinematics and Dynamics.* Oxford University Press, 431 pp.

Cassano, J. J., E. N. Cassano, M. W. Seefeldt, W. J. Gutowski Jr., and J. M. Glisan, 2016: Synoptic Conditions during Wintertime Temperature Extremes in Alaska. *J. Geophys. Res.*, **121**, 3241–3262, doi: 10.1002/2015JD024404.

Charles, M. E. and B. A. Colle, 2009: Verification of Extratropical Cyclones within the NCEP Operational Models. Part I: Analysis Errors and Short-Term NAM and GFS Forecasts. *Wea. Forecasting*, **24**, 1173–1190, doi: 10.1175/2009WAF2222169.1.

Colman, B. R., and C. F. Dierking, 1992: The Taku Wind of Southeast Alaska: Its Identification and Prediction, *Wea. Forecasting*, **7**, 49–64, doi: 10.1175/1520-0434(1992)007<0049:TTWOSA>2.0.CO;2.

Colucci, S. J. and L. F. Bosart, 1979: Surface Anticyclone Behavior in NMC Prediction Models. *Mon. Wea. Rev.*, **107**, 377–394, doi: 10.1175/1520-0493(1979)107<0377:SABINP>2.0.CO;2.

Cullather, R. I., Y. K. Lim, L. N. Boisvert, L. Brucker, J. N. Lee, and S. M. J. Nowicki, 2016: Analysis of the Warmest Arctic Winter, 2015-2016. *Geophys. Res. Lett.*, **43**, 10, 808–816, doi:10.1002/2016GL071228.

Crosman, E., and J. Horel, 2016: Winter Lake Breezes near the Great Salt Lake. *Boundary Layer Meteor.* **159**, 439–464, doi:10.1007/s10546-015-0117-6.

Gambacorta, A., and C. D. Barnet, 2013: Methodology and Information Content of the NOAA NESDIS Operational Channel Selection for the Cross-Track Infrared Sounder (CrIS). *IEEE Trans. Geosci. Remote Sens.*, **51**, 3207-3216, doi: 10.1109/tgrs.2012.2220369.

Grice, G. K., and A. L. Comisky, 1976: Thunderstorm climatology of Alaska. NOAA Tech. Memo. NWS AR-14, 36 pp. [Available online at https://docs.lib.noaa.gov/noaa_documents/NWS/TM_NWS_AR/TM_NWS_AR_14.PDF]

Holton, J. R., and G. J. Hakim, 2012: *An Introduction to Dynamic Meteorology* (5th ed.). Academic Press, 532 pp.

Horel, J., M. Splitt, L. Dunn, J. Pechmann, B. White, C. Ciliberti, S. Lazarus, J. Slemmer, D. Zaff, and J. Burks, 2002: Mesowest: Cooperative Mesonets in the Western United States. *Bull. Amer. Meteor. Soc.*, **83**, 211–225, doi: 10.1175/1520-0477(2002)083<0211:MCMITW>2.3.CO;2.

Horel, J. and B. Colman, 2005: Real-time and Retrospective Mesoscale Objective

Analyses. *Bull. Amer. Meteor. Soc.*, **86**, 1477–1480, doi: 10.1175/BAMS-86-10-1477.

Hopkins, R. H., 1994: Anchorage Windstorm of 1 December 1992. *Wea. Forecasting*, **9**, 469–478, doi: 10.1175/1520-0434(1994)009<0469:AWOD>2.0.CO;2.

Jacques, A. A., J. D. Horel, E. T. Crosman, and F. L. Vernon, 2015: Central and Eastern United States Surface Pressure Variations Derived from the USArray Network. *Mon. Wea. Rev.*, **143**, 1472–1493, doi: 10.1175/MWR-D-14-00274.1.

Jacques, A. A., J. D. Horel, E. T. Crosman, F. Vernon, and J. Tytell, 2016: The Earthscope US Transportable Array 1 Hz Surface Pressure Dataset. *Geosciences Data Journal*, **3**, 29–36, doi: 10.1002/gdj3.37.

Jacques, A. A., J. D. Horel, E. T. Crosman, and F. L. Vernon, 2016: EarthScope USArray Transportable Array (TA) Surface Pressure Observations Sampled at 1 Hz Frequency. *Research Data Archive at the National Center for Atmospheric Research, Computational and Information Systems Laboratory*. doi: 10.5065/D6028PRS.

Jacques, A. A., J. D. Horel, E. T. Crosman, and F. L. Vernon, 2017: Tracking Mesoscale Pressure Perturbations Using the USArray Transportable Array. Monthly Weather Review, In Press, doi: 10.1175/MWR-D-16-0450.1.

Kalnay, E., M. Kanamitsu, R. Kistler, W. Collins, D. Deaven, L. Gandin, M. Iredell, S. Saha, G. White, J. Woollen, Y. Zhu, A. Leetmaa, R. Reynolds, M. Chelliah, W. Ebisuzaki, W. Higgins, J. Janowiak, K. C. Mo, C. Ropelewski, J. Wang, R. Jenne, and D. Joseph, 1996: The NCEP/NCAR 40-Year Reanalysis Project. *Bull. Amer. Meteor. Soc.*, **77**, 437–471, doi: 10.1175/1520-0477(1996)077<0437:TNYRP>2.0.CO;2.

Kleist, D.T., D.F. Parrish, J.C. Derber, R. Treadon, W. Wu, and S. Lord, 2009: Introduction of the GSI into the NCEP Global Data Assimilation System. *Wea. Forecasting*, **24**, 1691–1705, doi: 10.1175/2009WAF2222201.1.

Lin, H., S. S. Weygandt, S. G. Benjamin, and M. Hu, 2017: Satellite Radiance Data Assimilation within the Hourly Updating Rapid Refresh. *Wea. Forecasting*, **32**, 1273–1287, doi: 10.1175/WAF-D-16-0215.1.

Liu, Q., W. Wolf, T. Reale, A. Sharma and NOAA JPSS Program Office, 2014: NESDIS-Unique CrIS-ATMS Product System (NUCAPS) Cloud-Cleared Radiances. Environmental Data Records. *NOAA National Centers for Environmental Information*, doi: 10.7289/V5WM1BG5.

Madaus, L. E., G. J. Hakim, C. F. Mass, 2014: Utility of Dense Pressure Observations for Improving Mesoscale Analyses and Forecasts. *Mon. Wea. Rev.*, **142**, 2398-2413,

doi: 10.1175/MWR-D-13-00269.1.

McMurdie, L. A. and J. H. Casola, 2009: Weather Regimes and Forecast Errors in the Pacific Northwest. *Wea. Forecasting*, **24**, 829–842, doi: 10.1175/2008WAF2222172.1.

Mesquita, M. S., D. E. Atkinson, and K. I. Hodges, 2010: Characteristics and Variability of Storm Tracks in the North Pacific, Bering Sea, and Alaska. *J. Climate*, **23**, 294–311, doi: 10.1175/2009JCLI3019.1.

Mohr, M., 2004: Problems with the Mean Sea Level Pressure Field over the Western United States. *Mon. Wea. Rev.*, **132**, 1952-1965, doi: 10.1175/1520-0493(2004)132<1952:PWTMSL>2.0.CO;2.

Murray, M. J., 1956: Strong Surface Winds at Big Delta, Alaska. *Mon. Wea. Rev.*, **84**, 15–24, doi: 10.1175/1520-0493(1956)084<0015:SSWABD>2.0.CO;2.

Nalli, N. R., C. D. Barnet, A. Reale, D. Tobin, A. Gambacorta, E. S. Maddy, E. Joseph, B. Sun, L. Borg, A. K. Mollner, V. R. Morris, X. Liu, M. Divakarla, P. J. Minnett, R. O. Knuteson, T. S. King, andW. W. Wolf, 2013: Validation of Satellite Sounder Environmental Data Records: Application to the Cross-Track Infrared Microwave Sounder Suite. *J. Geophys. Res.*, **118**, 13628-13643, doi: 10.1002/2013jd020436.

Nance, L.B. and B.R. Colman, 2000: Evaluating the Use of a Nonlinear Two-Dimensional Model in Downslope Windstorm Forecasts. *Wea. Forecasting*, **15**, 715–729, doi: 10.1175/1520-0434(2000)015<0715:ETUOAN>2.0.CO;2.

Overland, J. E. and N. Bond, 1993: The Influence of Coastal Orography: The Yakutat Storm. *Mon. Wea. Rev.*, **121**, 1388–1397, doi: 10.1175/1520-0493(1993)121<1388:TIOCOT>2.0.CO;2.

Papineau, J. M., 2001: Wintertime Temperature Anomalies in Alaska Correlated with ENSO and PDO. *Int. J. Climatol.*, **21**, 1577–1592, doi: 10.1002/joc.686.

Partain, J. L., S. Alden, H. Strader, U. S. Bhatt, P. A. Bieniek, B. R. Brettschneider, J. E. Walsh, R. T. Lader, P. Q. Olsson, T. S. Rupp, R. L. Thoman, A. D. York, and R. H. Ziel, 2016: An Assessment of the Role of Anthropogenic Climate Change in the Alaska Fire Season of 2015. *Bull. Amer. Meteor. Soc.*, **97**, S14–S18, doi: 10.1175/BAMS-D-16-0149.1.

Pauley, P. M., 1998: An Example of Uncertainty in Sea Level Pressure Reduction. *Wea. Forecasting*, **13**, 833–850, doi: 10.1175/1520-0434(1998)013<0833:AEOUIS>2.0.CO;2.

Pavlis, G. L., K. Sigloch, S. Burdick, M. J. Fouch, and F. L. Vernon, 2012: Unraveling

the Geometry of the Farallon Plate: Synthesis of Three-Dimensional Imaging Results from USArray. *Tectonophysics*, **532**, 82–102, doi: 10.1016/j.tecto.2012.02.008.

Pickart, R. S., A. M. Macdonald, G. W. K. Moore, I. A. Renfrew, J. E. Walsh, and W. S. Kessler, 2009: Seasonal Evolution of Aleutian Low Pressure Systems: Implications for the North Pacific Subpolar Circulation. *J. Phys. Oceanogr.*, **39**, 1317–1339, doi: 10.1175/2008JPO3891.1.

Reap, R. M., 1991: Climatological Characteristics and Objective Prediction of Thunderstorms over Alaska. *Wea. Forecasting,* **6**, 309–319, doi: 10.1175/1520-0434(1991)006<0309:CCAOPO>2.0.CO;2.

Rodionov, S. N., J. E. Overland, and N. A. Bond, 2005: The Aleutian Low and Winter Climatic Conditions in the Bering Sea. Part I: Classification. *J. Climate*, **18**, 160-177, doi:10.1175/JCLI3253.1.

Searby, H. W., 1968: Climate of the States: Alaska. U.S. Dept. of Commerce ESSA Weather Bureau Rep. 60–49, 23 pp.

Shulski, M., and G. Wendler, 2007: *The Climate of Alaska.* University of Alaska Press, 216 pp.

Shulski, M., J. Walsh, E. Stevens, and R. Thoman, 2010: Diagnosis of Extended Cold-Season Temperature Anomalies in Alaska. *Mon. Wea. Rev.,* **138**, 453–462, doi:10.1175/2009MWR3039.1.

Skamarock, W. C., and Coauthors, 2008: A description of the Advanced Research WRF version 3. NCAR Tech. Note NCAR/TN-475+STR, 113 pp. [Available online at http://www2.mmm.ucar.edu/wrf/users/docs/arw_v3.pdf.].

Smirnova, T.G., J.M. Brown, S.G. Benjamin, and J.S. Kenyon, 2016: Modifications to the Rapid Update Cycle Land Surface Model (RUC LSM) Available in the Weather Research and Forecasting (WRF) Model. *Mon. Wea. Rev.*, **144**, 1851–1865, doi: 10.1175/MWR-D-15-0198.1.

Smith, W. L., H. Revercomb, G. Bingham, A. Larar, H. Huang, D.Zhou, J. Li, X. Liu, and S. Kireev, 2009: Technical Note: Evolution, Current Capabilities, and Future Advances in Satellite Nadir Viewing Ultra-spectral IR Soundings of the Lower Atmosphere, *Atmos. Chem. Phys*, **9**,5563–5574, doi:10.5194/acp-9-5563-2009.

Thompson, D. W. J., and J. M. Wallace, 1998: The Arctic Oscillation Signature in the Wintertime Geopotential Height and Temperature Fields. *Geophys. Res. Lett.*, **25**, 1297–1300, doi:10.1029/98GL00950.

Thompson, G. and T. Eidhammer, 2014: A Study of Aerosol Impacts on Clouds and

Precipitation Development in a Large Winter Cyclone. *J. Atmos. Sci.*, **71**, 3636–3658, doi: 10.1175/JAS-D-13-0305.1.

Tyndall, D. P. and J. D. Horel, 2013: Impacts of Mesonet Observations on Meteorological Surface Analyses. *Wea. Forecasting*, **28**, 254–269, doi: 10.1175/WAF-D-12-00027.1.

Tytell, J., F. Vernon, M. Hedlin, C. de Groot Hedlin, J. Reyes, B. Busby, K. Hafner, and J. Eakins, 2016: The USArray Transportable Array as a Platform for Weather Observation and Research. *Bull. Amer. Meteor. Soc.*, **97**, 603–619, doi: 10.1175/BAMS-D-14-00204.1.

Wallace, J. M., and P. V. Hobbs, 2006: *Atmospheric Science, An Introductory Survey* (2nd ed.). Academic Press, 504 pp.

Walsh, J. E., P. A. Bieniek, B. Brettschneider, E. S. Euskirchen, R. Lader, and R. L. Thoman, 2017: The Exceptionally Warm Winter of 2015/16 in Alaska. *J. Climate*, **30**, 2069–2088, doi:10.1175/JCLI-D-16-0473.1.

Wheatley, D. M., and D. J. Stensrud, 2010: The Impact of Assimilating Surface Pressure Observations on Severe Weather Events in a WRF Mesoscale Ensemble System. *Mon. Wea. Rev.*, **138**, 1673-1694.

Whitaker, J. S., T. M. Hamill, X. Wei, Y. Song, and Z. Toth, 2008: Ensemble Data Assimilation with the NCEP Global Forecast System. *Mon. Wea. Rev.*, **136**, 463–482, doi: 10.1175/2007MWR2018.1.

Wilson, J. G., and J. E. Overland, 1986: Meteorology. *The Gulf of Alaska, Physical Environment and Biological Resources*, D. W. Hood and S. T. Zimmerman, Eds., Alaska Office, Ocean Assessments Division, National Oceanic and Atmospheric Administration, U.S. Department of Commerce, 655 pp.

Wu, W. S., R. J. Purser, and D. F. Parrish, 2002: Three-Dimensional Variational Analysis with Spatially Inhomogeneous Covariances. *Mon. Wea. Rev.*, **130**, 2905–2916, doi: 10.1175/1520-0493(2002)130<2905:TDVAWS>2.0CO:2.

Yang, Y., and M. H. Ritzwoller, 2008: Teleseismic Surface Wave Tomography in the Western US Using the Transportable Array Component of USArray. *Geophys. Res. Lett.*, **35**, L04308, doi: 10.1029/2007GL032278.